







Forecasting Rates of Volcanic Activity on Terrestrial Exoplanets and Implications for Cryovolcanic Activity on Extrasolar Ocean Worlds

Lynnae C. Quick¹ , Aki Roberge¹ , Amy Barr Mlinar² , and Matthew M. Hedman³ 
¹NASA Goddard Space Flight Center, 8800 Greenbelt Road, Greenbelt, MD, 20771, USA; Lynnae.C.Quick@nasa.gov
²Planetary Science Institute, 1700 East Fort Lowell Road, Tucson, AZ 85719, USA
³University of Idaho, Department of Physics, 875 Perimeter Drive, Moscow, ID 83844, USA
Received 2019 October 30; accepted 2020 May 20; published 2020 June 18

Abstract

Like the planets and moons in our solar system, the surfaces of terrestrial exoplanets may be shaped by volcanic activity. The magnitudes and rates of volcanic activity on terrestrial exoplanets will be intimately linked to their sizes and internal heating rates and can either facilitate or preclude the existence of habitable environments. In order to place bounds on the potential for such activity, we estimate total internal heating rates for 53 exoplanets with masses and radii up to $\sim 8M_{\oplus}$ and $2R_{\oplus}$, respectively, assuming that internal heating is drawn from both radiogenic and tidal sources. We then compare these internal heating rates to those of the planets and moons in our solar system in an attempt to constrain the expected rates of volcanic activity on these extrasolar worlds. We find that all 53 of the exoplanets surveyed are likely to have volcanic activity at their surfaces, and that at least 26% of these planets may be extrasolar ocean worlds. The majority of these ocean worlds may be similar in structure to the icy moons of the giant planets, having internal oceans beneath layers of surface ice. If so, these planets may exhibit cryovolcanism (i.e., icy volcanism) at their surfaces. Recent studies have shown that extrasolar volcanism could be detected by high-resolution spectrographs on existing ground-based telescopes. In the case of planets with densities and/or effective temperatures that are consistent with H_2O -rich compositions, spectral identification of excess water vapor and other molecules that are explosively vented into space during cryovolcanic eruptions could serve as a way to infer the presence of subsurface oceans, and therefore indirectly assess their habitability. Considering the implications for habitability, our results suggest that continued characterization of terrestrial exoplanets in terms of their potential for volcanic activity should be a priority in the coming years.

Key words: Exoplanet atmospheres – Exoplanet structure – Exoplanet surface characteristics – Exoplanets – Exosphere – Extrasolar rocky planets – Ocean planets – Tidal friction – Volcanoes

Online material: color figures

1. Introduction

Primitive atmospheres on rocky planets are formed from volatiles that are outgassed during their magma ocean phase. Rocky planets may experience numerous magma ocean phases during their early evolution; these phases may develop as a result of impacts (Tonks & Melosh 1993), potential energy release during core formation (Sasaki & Nakazawa 1986), or radiogenic heating (Elkins-Tanton 2012). Planetary evolution is fundamentally tied to the evolution of magma oceans as processes that take place during magma ocean crystallization determine a planet's tectonic behavior, initial chemical and thermal structure, and atmospheric composition (Massol et al. 2016; Ikoma et al. 2018; Kite et al. 2020). For example, degassing of the lunar magma ocean after the Moon-forming impact may have produced a short-lived metal atmosphere on the Moon's Earth-facing side; this early lunar atmosphere may be analogous to atmospheres that exist on young,

close-in rocky exoplanets with global magma oceans (Saxena et al. 2017).

Notwithstanding, primitive atmospheres formed from magma ocean degassing are likely to be stripped from close-in planets by stellar winds and CMEs (Khodachenko et al. 2007; Kite et al. 2009). Volcanic outgassing will facilitate the formation of secondary atmospheres on these worlds. Conversely, a lack of volcanism, or infrequent volcanic events, would preclude a rocky planet from maintaining an atmosphere. On stagnant-lid planets, the lack of substantial CO_2 -rich atmospheres would drive surface temperatures down, making them too cool to maintain liquid water at their surfaces, thereby reducing the widths of habitable zones in their respective systems (Kadoya & Tajika 2014; Noack et al. 2014, 2017; Abbot 2016). For this reason, geologically active planets that host frequent volcanic eruptions may represent more favorable habitable environments than planets on which volcanic events are sporadic or non-existent (Misra et al. 2015). In the case of

cold, cryovolcanically-active exoplanets, the detection of eruptive activity could signify the presence of internal oceans and near-surface habitable niches, as is the case for several icy moons in our solar system. Volcanism is therefore intimately linked to planetary habitability.

Owing to their bright infrared flux and short orbital periods, volcanic exoplanets and exoplanets with global magma oceans may be among the most detectable and characterizable low-mass exoplanets in the coming decades (Henning et al. 2018). Recent studies have attempted to characterize volcanic activity on rocky extrasolar worlds using transmission and UV spectroscopy, and with eclipse observations. These studies have shown that while plasma tori surrounding volcanically-active exoplanets could be detected by Hubble Space Telescope UV observations (Kislyakova et al. 2019), eclipse observations could be used to characterize the variability in activity on highly volcanic exoplanets (Tamburo 2018). In addition, by modeling high-resolution alkali spectra, Oza et al. (2019) have demonstrated that volcanic activity may be prevalent on exomoons orbiting close-in gas giant exoplanets. In exploring the lifetime and spectral evolution of magma oceans on Earth-sized terrestrial planets, Hamano et al. (2015) found that the thermal and spectral evolution of magma oceans on these bodies is dependent upon their distance from the host star, with close-in planets producing strong enough thermal radiation to be detectable for the entire lifetime of the magma ocean, while thermal radiation from planets at farther orbital distances would sharply decrease within 10^6 yr. Neglecting internal heat sources, Bonati et al. (2019) found that magma oceans may persist from 10^2 – 3×10^6 yr on newly formed planets. These authors also found that owing to their molten surfaces, young planets with magma oceans may be directly imaged at infrared wavelengths by space-based interferometers or high-resolution ground-based telescopes. Similarly, the high albedos of icy, cryovolcanically active worlds will make them far more detectable than rocky planets in reflected light (see Wolf 2017). Detections of volcanic activity on these far-away worlds would allow for the examination of their internal structures and compositions from afar.

While volcanism can indeed induce habitable environments on low-mass exoplanets (e.g., Ramirez & Kaltenegger 2017), excessive volcanism (see Demory et al. 2015) would produce unstable surface environments that could render exoplanets incapable of hosting life (Jackson et al. 2008). The frequency and relative strength of volcanic activity on extrasolar planets will therefore directly affect their habitability. The prevalence of volcanic activity on terrestrial exoplanets is intimately linked to the thermal states of these worlds (Dorn et al. 2018). In order to gauge the habitability of terrestrial exoplanets, including the potential for reservoirs of liquid water on volatile-rich planets, it is therefore necessary to constrain the amount of volcanic or

cryovolcanic activity that may be occurring at their surfaces. While the identification of gas and dust produced by active eruptions is one way to identify volcanically active extrasolar worlds (see Guenther et al. 2011; Misra et al. 2015; Arkhyrov et al. 2019), our first step is to determine which exoplanets are likely to be volcanically or cryovolcanically active based on their internal heating rates. Dorn et al. (2018) explored volcanic outgassing of CO_2 on rocky exoplanets with stagnant lids that ranged from 1 to $8M_{\oplus}$. They found that planets between 2 and $3 M_{\oplus}$ are most likely to be volcanically active. Kite et al. (2009) explored rates of volcanism as a function of planet mass and time for terrestrial exoplanets between 0.25 and $25M_{\oplus}$. However, their analysis did not consider the effects of tidal heating on volcanic activity.

Here, we provide rough estimates for the total internal heating rates of 53 low-mass exoplanets, with masses between 0.086 and $8M_{\oplus}$ and radii between 0.54 (Mars-sized) and $2R_{\oplus}$ assuming that these planets are primarily heated by radiogenic and tidal sources. We then use these results to constrain rates of (cryo)volcanic activity at their surfaces, employing activity rates for the planets and moons in our solar system as a baseline. We have surveyed exoplanets that are up to $8M_{\oplus}$ and $2R_{\oplus}$ in an effort to ensure that we capture Corot-7b, which is likely very volcanically active (Barnes et al. 2010; Léger et al. 2011), along with recently discovered planets such as Pi Mensae c (Huang et al. 2018), and low-density exoplanets such as Kepler 60 c & d (Jontof-Hutter et al. 2016) in our analyses. Notwithstanding, the overwhelming majority of the exoplanets we have surveyed have radii $\leq 1.7R_{\oplus}$ (Table 1). This was done to ensure that the exoplanets considered here are indeed super-Earths rather than mini-Neptunes (Owen & Wu 2017; Fulton & Petigura 2018; Mordasini 2020).

2. Methods

All of the geological activity on the planets and moons in our solar system is driven by internal heating. On Earth, the Moon, and the terrestrial planets, geological processes are driven by radiogenic heating. However on the moons of the giant planets such as Io, Enceladus and Europa, geological processes are primarily driven by tidal heating (Cassen et al. 1979; Peale et al. 1979; Hurford et al. 2007; Meyer & Wisdom 2007; Nimmo et al. 2007; Roberts & Nimmo 2008; Tobie et al. 2008). Terrestrial exoplanets (Jackson et al. 2008; Henning & Hurford 2014; Driscoll & Barnes 2015; Barr et al. 2018; Makarov et al. 2018; Hurford et al. 2020) and exomoons (Scharf 2006; Cassidy et al. 2009; Oza et al. 2019) may also experience geological activity as a result of tidal heating from their primaries and due to the decay of radioactive elements in their interiors (Frank et al. 2014). We therefore assume that volcanic activity on terrestrial exoplanets is driven by both tidal and radiogenic heating.

Table 1
Solar System and Extrasolar Planetary Parameters [1 W = 10^7 erg s $^{-1}$] SI = Super-Io; Mow = Magma Ocean World; EVP = Exo-Venus Planet; SE = Super-Europa/Super-Enceladus Planet; ST = Super-Triton

World	$R_p (R_{\oplus})$	$M_p (M_{\oplus})$	ρ (kg m $^{-3}$)	g (m s $^{-2}$)	T_{EFF}/T_S^a (K)	System		$H_{\text{Radiogenic}}$ (W)	H_{Tidal} (W)	H_{Total} (W)	Type	References
						Age (Gyr)	$255 (T_{\text{EFF}}) 288(T_S)$					
Earth	1	1	5500	9.8	255 (T_{EFF}) 288(T_S)	4.5	4×10^{13}	... ^b	4.7×10^{13}	rocky	Turcotte (1995), Turcotte & Schubert (2002)	
Venus	0.82	0.95	5240	8.87	260 K (T_{EFF}) 737 (T_S)	4.5	2.91×10^{13}	...	2.91×10^{13}	rocky	Turcotte (1995), Schubert et al. (1997)	
Early Venus	0.82	0.95	5240	8.87	?	4	2×10^{14}	...	2×10^{14}	rocky	Turcotte (1995)	
Io	0.286	0.015	3528	1.8	110	4.5	3.7×10^{11}	1×10^{14}	1×10^{14}	rocky	Yoder & Peale (1981), Schubert et al. (2004), Hussmann & Spohn (2004)	
Europa	0.245	0.008	3000	1.31	100	4.5	2.1×10^{11}	1×10^{12}	1.21×10^{12}	icy	Schubert et al. (2004), Hussmann & Spohn (2004), ^c Chen et al. (2014), Quick & Marsh (2015)	
Enceladus	0.0395	1.8×10^{-5}	1610	0.11	75	4.5	2.73×10^8	1.6×10^{10}	1.63×10^{10}	icy	Howett et al. (2011), ^c Chen et al. (2014)	
Triton	0.21	0.00359	2060	0.78	38	4.5	7.12×10^{10}	6.6×10^{10}	1.37×10^{11}	icy	Gaeman et al. (2012), ^c Chen et al. (2014) and references therein	
Callisto	0.378	0.018	1834	1.235	126	4.5	3.2×10^{11}	3.3×10^9	3.2×10^{11}	icy	Moore & Schubert (2003), ^c Chen et al. (2014) and (1)	
Ganymede	0.413	0.025	1942	1.43	117	4.5	4.67×10^{11}	1.1×10^{10}	4.78×10^{11}	icy	Moore & Schubert (2003), Schubert et al. (2004), ^c Chen et al. (2014) and (1)	
Titan	0.404	0.0225	2575	1.35	94	4.5	4.11×10^{11}	8.75×10^{10}	4.99×10^{11}	icy	^c Chen et al. (2014), Schubert et al. (1986) and (1)	
Mercury	0.38	0.055	5427	3.7	440	4.5	2.25×10^{12}	1.4×10^9	2.25×10^{12}	rocky	Peplowski et al. (2011), Makarov & Efroimsky (2014), Ogawa (2016), ^c	
Early Mercury	0.38	0.055	5427	3.7	?	4	3.2×10^{12}	...	3.2×10^{12}	rocky	Hauck et al. (2004), Breuer et al. (2007)	

Table 1
(Continued)

World	$R_P (R_{\oplus})$	$M_P (M_{\oplus})$	ρ (kg m ⁻³)	g (m s ⁻²)	$T_{\text{EFF}}/T_{\text{S}}^a$ (K)	System Age (Gyr)	$H_{\text{Radiogenic}}$ (W)	H_{Tidal} (W)	H_{Total} (W)	Type	References
Mars	0.533	0.107	3934	3.72	210	4.5	2.74×10^{12}	1×10^9	2.74×10^{12}	rocky	Parro et al. (2017), Manga et al. (2019)
The Moon	0.273	0.012	3344	1.62	215(equator) 104 (poles)	4.5	3×10^{11}	...	3×10^{11}	rocky	Siegler & Smrekar (2014), Paige & Siegler (2016), Williams et al. (2017)
Early Moon	0.273	0.012	3344	1.62	?	0.1	1.15×10^{12}	1.05×10^{12}	2.2×10^{12}	rocky	Meyer et al. (2010), Frank et al. (2014)
Pluto	0.1868	2.18×10^{-3}	1854	0.620	44	4.5	5.32×10^{10}	...	5×10^{10}	icy	Robuchon & Nimmo (2011), McKinnon et al. (2016)
Charon	0.095	2.7×10^{-4}	1702	0.288	53	4.5	4.4×10^9	...	4.4×10^9	icy	Hussmann et al. (2006), Cook et al. (2007)
Ceres	0.074	1.5×10^{-4}	2160	0.28	150	4.5	4.5×10^9	...	4.5×10^9	ice/rock hybrid	Castillo-Rogez et al. (2019)
Miranda	0.037	1.1×10^{-5}	1200	0.079	60	4.5	8.5×10^7	...	8.5×10^7	icy	^c Chen et al. (2014)
Ariel	0.091	2.3×10^{-4}	1592	0.269	60	4.5	3.6×10^9	...	3.6×10^9	icy	^c Chen et al. (2014)
Rhea	0.12	3.9×10^{-4}	1233	0.264	99 (dayside) 53(nightside)	4.5	3.3×10^9	...	3.3×10^9	icy	^c Chen et al. (2014)
Mimas	0.03	6.3×10^{-6}	1148	0.064	64	4.5	4×10^7	2.9×10^8	3.3×10^8	icy	^c Chen et al. (2014)
Dione	0.09	1.8×10^{-4}	1480	0.232	87	4.5	2.46×10^9	...	2.46×10^9	icy	^c Chen et al. (2014)
55 Cancri e	1.91	8.08	6400	21.7	1958	10.2	1.14×10^{14}	4.28×10^{21}	4.28×10^{21}	rocky (MOW)	Demory et al. (2011, 2015, 2016)
Corot 7 b	1.55	5.7	7500	23	1756	1.32	2.17×10^{14}	0 ($e = 0$)	2.17×10^{14}	rocky (MOW)	Queloz et al. (2009), Barros et al. (2014), Stassun et al. (2017)
GJ 1132 b	1.13	1.66	6300	12.9	529	5	3.66×10^{13}	TBD: e unknown	3.66×10^{13}	rocky (EVP)	Berta-Thompson et al. (2015), Bonfils et al. (2018), Dittmann et al. (2017a)
HD 219134 b	1.6	4.74	6340	18	1015	11	6.42×10^{13}	0 ($e = 0$)	6.42×10^{13}	rocky (MOW)	Gillon et al. (2017a)
HD 219134c	1.5	4.36	6950	18.7	782	11	5.39×10^{13}	2.17×10^{16}	2.17×10^{16}	Rocky (SI)	Gillon et al. (2017a)
^g HD 219134 f	1.31	unknown	unknown	unknown	522	11	3.51×10^{13}	1.42×10^{14}	1.77×10^{14}	unknown	Gillon et al. (2017a)

4

Table 1
(Continued)

World	$R_P (R_{\oplus})$	$M_P (M_{\oplus})$	ρ (kg m ⁻³)	g (m s ⁻²)	T_{EFF}/T_s^a (K)	System Age (Gyr)	$H_{\text{Radiogenic}}$ (W)	H_{Tidal} (W)	H_{Total} (W)	Type	References
HD 3167 b	1.7	5.02	5600	17	1669	7.8	9.49×10^{13}	0 ($e = 0$)	9.49×10^{13}	rocky (MOW)	Christiansen et al. (2017), Livingston et al. (2018)
Kepler 10 b	1.45	4.6	8255	21	2130	10.6	4.9×10^{13}	TBD: e unknown	4.91×10^{13}	rocky (MOW)	Esteves et al. (2015)
Kepler 11 b	1.8	1.9	1720	5.7	unknown	8.5	1.07×10^{14}	^h 1.12×10^{15}	1.23×10^{15}	cold ocean planet	Lissauer et al. (2013), Borsato et al. (2014)
Kepler 21 b	1.61	5.09	6720	19	2025	3.03	1.48×10^{14}	2.6×10^{17}	2.6×10^{17}	rocky (MOW)	López-Morales et al. (2016)
Kepler 36 b	1.46	4.45	7810	20	978	6.8	6.6×10^{13}	2×10^{14}	2.7×10^{14}	rocky (MOW)	Carter et al. (2012)
Kepler 60 b	1.68	4.2	4620	14	unknown	5.1	1.3×10^{14}	9.4×10^{14}	1.1×10^{15}	ocean planet	Gozdziewski et al. (2016), Jontof-Hutter et al. (2016), Morton et al. (2016)
Kepler 60 c	1.9	3.85	3060	10.4	unknown	5.1	1.7×10^{14}	3.81×10^{15}	3.98×10^{15}	cold ocean planet	Gozdziewski et al. (2016), Jontof-Hutter et al. (2016), Morton et al. (2016)
Kepler 60 d	1.99	4.16	2910	10.3	unknown	5.1	1.97×10^{14}	3.03×10^{14}	5×10^{14}	cold ocean planet	Gozdziewski et al. (2016), Jontof-Hutter et al. (2016), Morton et al. (2016)
Kepler 62 c	0.54	unknown	unknown	unknown	578	7	3.16×10^{13}	TBD: e unknown	3.16×10^{13}	unknown	Borucki et al. (2013)
Kepler 68 c	0.96	2.04	unknown	21.7	unknown	6.3	1.94×10^{13}	0 ($e = 0$)	1.94×10^{13}	unknown	Berger et al. (2018), Mills et al. (2019)
Kepler 70 b	0.76	0.44	5528	7.5	unknown	unknown	TBD: system age unknown	TBD: e unknown	unknown	rocky	Charpinet et al. (2011)
Kepler 70 c	0.87	0.66	5521	8.5	unknown	unknown	TBD: system age unknown	TBD: e unknown	unknown	rocky	Charpinet et al. (2011)
Kepler 78 b	1.1	3.2	unknown	14	2250	0.75	9.57×10^{13}	TBD: e unknown	9.57×10^{13}	candidate rocky (MOW)	Pepe et al. (2013), Stassun et al. (2017)
Kepler 80 d	1.53	6.75	7040	28	720	2	1.55×10^{14}	TBD: e unknown	1.55×10^{14}	rocky (SI)	Muirhead et al. (2012), MacDonald et al. (2016)
Kepler 80 e	1.6	4.1	3750	16	628	2	1.8×10^{14}	TBD: e unknown	1.8×10^{14}	candi-date ocean planet	Muirhead et al. (2012), MacDonald et al. (2016)

Table 1
(Continued)

World	$R_P (R_{\oplus})$	$M_P (M_{\oplus})$	$\rho (\text{kg m}^{-3})$	$g (\text{m s}^{-2})$	$T_{\text{EFF}}/T_{\text{S}}^a (\text{K})$	System Age (Gyr)	$H_{\text{Radiogenic}} (\text{W})$	$H_{\text{Tidal}} (\text{W})$	$H_{\text{Total}} (\text{W})$	Type	References
Kepler 93 b	1.6	3.2	4292	12	1037	6.6	8.74×10^{13}	0 ($e = 0$)	8.74×10^{13}	candi-date ocean planet	Dressing et al. (2015), Stassun et al. (2017)
Kepler 97 b	1.5	3.5	5440	16	unknown	8.4	5.66×10^{13}	TBD: e unknown	5.66×10^{13}	rocky	Marcy et al. (2014)
Kepler 99 b	1.5	6.2	10900	28	unknown	1.5	1.66×10^{14}	TBD: e unknown	1.66×10^{14}	rocky	Marcy et al. (2014)
Kepler 100 b	1.3	7.3	14250	42.5	unknown	6.5	4.7×10^{13}	TBD: e unknown	4.7×10^{13}	rocky	Marcy et al. (2014)
Kepler 101 c	1.2	unknown	unknown	unknown	1412	5.9	4.3×10^{13}	0 ($e = 0$)	4.3×10^{13}	candi-date rocky (MOW)	Bonomo et al. (2014)
Kepler 102 d	1.2	3.8	13270	28	unknown	1.4	8.66×10^{13}	TBD: e unknown	8.66×10^{13}	rocky	Marcy et al. (2014)
Kepler 105 c	1.3	4.6	11200	27.3	997	3.5	6.85×10^{13}	TBD: e unknown	6.85×10^{13}	rocky (MOW)	Everett et al. (2015), Jontof-Hutter et al. (2016), Morton et al. (2016)
Kepler 114 c	1.6	2.8	4039	11.3	508	2.7	1.49×10^{14}	TBD: e unknown	1.49×10^{14}	candi-date ocean planet	Muirhead et al. (2012), Xie (2014), Morton et al. (2016)
Kepler 138 b	0.7	0.19	3020	3.8	unknown	4.7	9×10^{12}	5.33×10^{11}	9.5×10^{12}	cold ocean planet	Morton et al. (2016), Almenara et al. (2018)
Kepler 138 c	1.7	5.2	6100	18.3	398	4.7	1.3×10^{14}	3.2×10^{13}	1.6×10^{14}	candi-date ocean planet	Muirhead et al. (2012), Morton et al. (2016), Almenara et al. (2018)
Kepler 138 d	1.7	1.2	1360	4	335	4.7	1.3×10^{14}	1.5×10^{13}	1.4×10^{14}	ocean planet	Muirhead et al. (2012), Morton et al. (2016), Almenara et al. (2018)
Kepler 186 b	1.07	unknown	unknown	unknown	579	4	3.6×10^{13}	TBD: e unknown	3.6×10^{13}	unknown	Muirhead et al. (2012), Quintana et al. (2014), Torres et al. (2015)
Kepler 186 c	1.25	unknown	unknown	unknown	470	4	5.7×10^{13}	TBD: e unknown	5.7×10^{13}	unknown	Muirhead et al. (2012), Quintana et al. (2014), Torres et al. (2015)
Kepler 186 d	1.4	unknown	unknown	unknown	384	4	8×10^{13}	TBD: e unknown	8×10^{13}	unknown	Muirhead et al. (2012),

Table 1
(Continued)

World	$R_p (R_{\oplus})$	$M_p (M_{\oplus})$	ρ (kg m ⁻³)	g (m s ⁻²)	T_{EFF}/T_s^a (K)	System Age (Gyr)	$H_{\text{Radiogenic}}$ (W)	H_{Tidal} (W)	H_{Total} (W)	Type	References
Kepler 186 e	1.27	unknown	unknown	unknown	unknown	4	6×10^{13}	TBD: e unknown	6×10^{13}	unknown	Quintana et al. (2014), Torres et al. (2015) Quintana et al. (2014), Torres et al. (2015)
Kepler 186 f	1.2	unknown	unknown	unknown	unknown	4	4.7×10^{13}	1.1×10^9	4.7×10^{13}	unknown	Torres et al. (2015)
Kepler 406 b	1.4	6.4	11820	30	unknown	5.8	6.8×10^{13}	TBD: e unknown	6.8×10^{13}	rocky	Marcy et al. (2014)
Kepler 406 c	0.85	2.7	24390	37	unknown	5.8	1.4×10^{13}	TBD: e unknown	1.4×10^{13}	rocky	Marcy et al. (2014)
Kepler 414 b	1.7	3.5	3845	11.7	unknown	5.5	1.14×10^{14}	TBD: e unknown	1.14×10^{14}	ocean planet	Hadden & Lithwick (2014), Morton et al. (2016)
L 98-59 b	0.8	0.5	5365	7.6	unknown	1 ⁱ	3.33×10^{13}	5.72×10^{17}	5.72×10^{17}	rocky	Kostov et al. (2019)
L 98-59 c	1.35	2.4	5358	12.9	unknown	1 ⁱ	1.6×10^{14}	5.38×10^{17}	5.38×10^{17}	rocky	Kostov et al. (2019)
L 98-59 d	1.57	3.4	4826	13.5	unknown	1 ⁱ	2.52×10^{14}	1.68×10^{17}	1.69×10^{17}	candi-date ocean planet	Kostov et al. (2019)
LHS 1140 b	1.73	6.98	7500	23	235	5 ^j	1.31×10^{14}	^k 6.15×10^{13}	1.93×10^{14}	cold ocean planet (SE)	Ment et al. (2019)
LHS 1140c	1.3	1.81	4700	10.8	438	5 ^j	5.34×10^{13}	^k 4.38×10^{18}	4.38×10^{18}	candi-date ocean planet (MOW)	Ment et al. (2019)
Pi Mensae c	2.04	4.82	2970	11.3	1169.8	2.98	3×10^{14}	0 ($e = 0$)	3×10^{14}	rocky	Huang et al. (2018)
Trappist-1 b	1.07	0.85	3400	7.3	400	8	2.3×10^{13}	7.02×10^{17}	7.02×10^{17}	candi-date ocean planet	Gillon et al. (2017b), Wang et al. (2017)
Trappist-1 c	1.04	1.38	7630	12.6	342	8	2.12×10^{13}	3.13×10^{16}	3.13×10^{16}	ocean planet	Wang et al. (2017)
Trappist-1 d	0.76	0.41	3950	7	288	8	8.29×10^{12}	2.3×10^{13}	3.13×10^{13}	ocean planet	Gillon et al. (2017b), Wang et al. (2017)
Trappist-1 e	0.9	0.64	1710	7.7	251	8	1.39×10^{13}	3.84×10^{13}	5.23×10^{13}	cold ocean planet (SE)	Gillon et al. (2017b), Wang et al. (2017)
Trappist-1 f	1.03	0.67	1740	6.2	219	8	2.05×10^{13}	2.31×10^{13}	4.36×10^{13}	cold ocean planet (SE)	Gillon et al. (2017b), Wang et al. (2017)
Trappist-1 g	1.11	1.34	2180	10.7	199	8	2.57×10^{13}	5.77×10^{11}	2.63×10^{13}	cold ocean	Wang et al. (2017)

Table 1
(Continued)

World	$R_p (R_\oplus)$	$M_p (M_\oplus)$	ρ (kg m ⁻³)	g (m s ⁻²)	T_{EFF}/T_S^a (K)	System Age (Gyr)	$H_{\text{Radiogenic}}$ (W)	H_{Tidal} (W)	H_{Total} (W)	Type	References
Trappist-1 h	0.72	0.086	1270	1.6	167	8	6.99×10^{12}	6.02×10^{12}	1.3×10^{13}	planet (ST) cold ocean planet (ST)	Wang et al. (2017)

Notes. In the case of non-transiting planets detected solely by the radial velocity technique, where only planet mass in terms of $m \sin i$ is known, we have assumed that planet mass, M_p , is equal to the minimum mass. Planet density, ρ , has been calculated for planets with an unknown bulk density using the relation: $\rho = 3M_p/4\pi R_p^3$. Similarly, surface gravity, g , has been calculated for planets for which surface gravity is unknown using $g = GM_p/R_p^2$.

^a T_S corresponds to the mean surface temperature of the planets and moons in our solar system.

^b Negligible tidal heating rate.

^c We have assumed that moons do not have a fully deformable interior (i.e., $k_2 \neq 1.5$).

^d H_{Tidal} for Triton corresponds to obliquity tides in the subsurface ocean, which contribute more internal energy than solid body tides. See Chen et al. (2014).

^e $H_{\text{Radiogenic}}$ for Mercury calculated using internal heating rate from Peplowski et al. (2011) and mantle mass from Ogawa (2016).

^f We have utilized radiogenic heating rates at 0.1 Gyr from Frank et al. (2014), and have calculated the mass of the lunar mantle, assuming that the radius and density of the mantle are 1.4×10^6 m and 3500 kg m^{-3} , respectively. This returns a mantle mass equal to 4×10^{22} kg for the Moon.

^g Smallest possible value of R_p from Gillon et al. (2017a).

^h In order to obtain a conservative tidal heating rate, we used the eccentricity value reported in Borsato et al. (2014) ($e = 0.026$) in Equation (1).

ⁱ Minimum stellar age from Kostov et al. (2019).

^j Minimum stellar age from Ment et al. (2019).

^k Eccentricity is poorly constrained; maximum eccentricity values substituted into (1). H_{Tidal} is preliminary.

If all energy imparted to a planet by tidal dissipation as it orbits its host star is dispersed as heat in the planet's interior, then the amount of heat imparted to the planet by tidal sources, H_{Tidal} , is well-represented by the energy dissipation, \dot{E} , and can be approximated as:

$$H_{\text{Tidal}} \sim \dot{E} = \frac{21}{2} \frac{k_2 \omega^5 R_p^5 e^2}{GQ} \quad (1)$$

(Roberts & Nimmo 2008; Quick & Marsh 2015; Barr et al. 2018). In Equation (1), k_2 is the degree 2 love number, which describes how the planet responds to the tide raised on it by its primary. k_2 ranges from 0 for a completely rigid planet, to 1.5 for a planet that is entirely fluid and therefore has a significant tidal response to the gravitational tug of its star. The quantity $\omega \approx \frac{2\pi}{T}$ is the planet's orbital mean motion, with orbital period T . R_p represents planet radius, and e is orbital eccentricity. Here G is the gravitational constant, and Q is the quality factor, which represents the fraction of energy that is dissipated as heat within the planet per orbital cycle. Q can range from 1 to 1×10^6 depending on a planet or moon's composition and internal structure (Goldreich & Soter 1966; Ojakangas & Stevenson 1989; Henning & Hurford 2014). A significant portion of tidal energy is dissipated as heat in the interiors of planets with high Q -values.

Frank et al. (2014) provide the radiogenic heating rate, per kg of mantle mass, (henceforth \dot{h}) in W kg^{-1} , for terrestrial exoplanets as a function of age, considering the radioactive isotopes ^{40}K , ^{232}Th , ^{235}U , and ^{238}U (this data is provided publicly in Supplementary Data 2 of Frank et al. 2014). Assuming that each planet's mantle makes up 84% of its total volume, as is the case for Earth (Stacey & Davis 2008), the volume of each planet's mantle, V_{mantle} , can be expressed as:

$$V_{\text{mantle}} = 0.84V_p = 0.84 \times \frac{4}{3}\pi R_p^3. \quad (2)$$

If we assume that the density of each planet's mantle, ρ_{mantle} , is 4000 kg m^{-3} , as is the case for Earth, (Stacey & Davis 2008), then the mass of each planet's mantle may be approximated by:

$$M_{\text{mantle}} = 0.84 \times \frac{4}{3}\pi R_p^3 \rho_{\text{mantle}}. \quad (3)$$

Upon obtaining \dot{h} from Frank et al. (2014) and assuming that the age of each exoplanet is identical to the average estimated age of its host star, the total radiogenic heating rate of each planet may be expressed as:

$$H_{\text{Radiogenic}} = \dot{h} M_{\text{mantle}}. \quad (4)$$

3. Results and Discussion

To demonstrate the utility of Equations (1) and (4), $H_{\text{Radiogenic}}$, H_{Tidal} , and H_{Total} , are listed along with physical and orbital parameters for 53 terrestrial exoplanets in Table 1. We considered planets with $M_p \leq 8M_{\oplus}$ and $R_p \leq 2R_{\oplus}$, which

ensures an Earth-like, rather than a sub-Neptune-like, composition (Stevenson 1982; Borucki et al. 2011; Fabrycky et al. 2014). In addition, we have utilized the relationship: $H_{\text{Total}} = H_{\text{Tidal}} + H_{\text{Radiogenic}}$ and assume that the planets do not have substantial bound atmospheres so that their average surface temperatures, T_S , may be taken to be equal to their effective temperatures, T_{EFF} . We have also substituted $k_2 = 0.3$, consistent with past studies of the terrestrial planets and icy moons in our solar system (Jackson et al. 2008; Kozai 1968; Quick & Marsh 2015; Hurford et al. 2020), and $Q = 100$, commensurate with past studies of tidal dissipation in our solar system's moons (e.g., Cassen et al. 1979; Peale et al. 1979; Chen et al. 2014; Quick & Marsh 2015) and the conservative end of studies that considered tidal dissipation in terrestrial exoplanets (Henning & Hurford 2014; Tamburo et al. 2018), into Equation (1). For comparison, Table 1 also includes H_{Total} , $H_{\text{Radiogenic}}$ and H_{Tidal} , along with physical parameters for the planets and moons in our solar system. In most cases, internal heating rates and physical parameters for the bodies in our solar system were extracted from the literature (Table 1 Refs. column). In cases where internal heating rates were not documented in the literature, they were calculated using the formulae introduced above. As is the case for the exoplanets in our study, these calculations assumed that solar system bodies are not fully deformable so that values of H_{Tidal} that are reflective of bodies with homogenous interiors and non-zero rigidities were adopted. (e.g., see Table 3 of Chen et al. 2014). Physical and orbital parameters for each exoplanet were extracted from the NASA Exoplanet Archive and from the references listed in Table 1.

We note that with H_{Total} on the order of 10^{14} W (Table 1), Io is the most volcanically active body in our solar system (Moore 2003; Lopes et al. 2004; McEwen et al. 2004). Further, volcanic activity is prevalent on Earth, which has $H_{\text{Total}} \sim 4 \times 10^{13} \text{ W}$ (Table 1) (Turcotte 1995; Turcotte & Schubert 2002), primarily due to radiogenic sources (Schubert et al. 1997; Turcotte & Schubert 2002). Volcanic activity was also widespread on early Venus (Turcotte 1995; Basilevsky et al. 1997; Schubert et al. 1997), which may have had H_{Total} as large as $2 \times 10^{14} \text{ W}$ (Turcotte 1995). Jupiter's icy moon Europa, which has $H_{\text{Total}} \sim 1 \text{ TW}$ (Chen et al. 2014; Quick & Marsh 2015), is also cryovolcanically and tectonically active (Fagents 2003; Kattenhorn & Hurford 2009; Prockter & Patterson 2009; Prockter et al. 2017; Quick et al. 2017b). Although explosive cryovolcanism on Europa may be periodic or transient in nature, and although this activity may display spatial variability (Roth et al. 2014a; Rhoden et al. 2015; Teolis et al. 2017b), the eruption of cold, geyser-like plumes has been inferred from multiple spectroscopic detections of water vapor and its constituent molecules emanating from the icy moon (Figure 1) (Roth et al. 2014b; Sparks et al. 2016, 2017; Paganini et al. 2019), as well as from in situ plasma wave and magnetic field observations by the Galileo spacecraft (Jia et al. 2018; Arnold et al. 2019, 2020). The

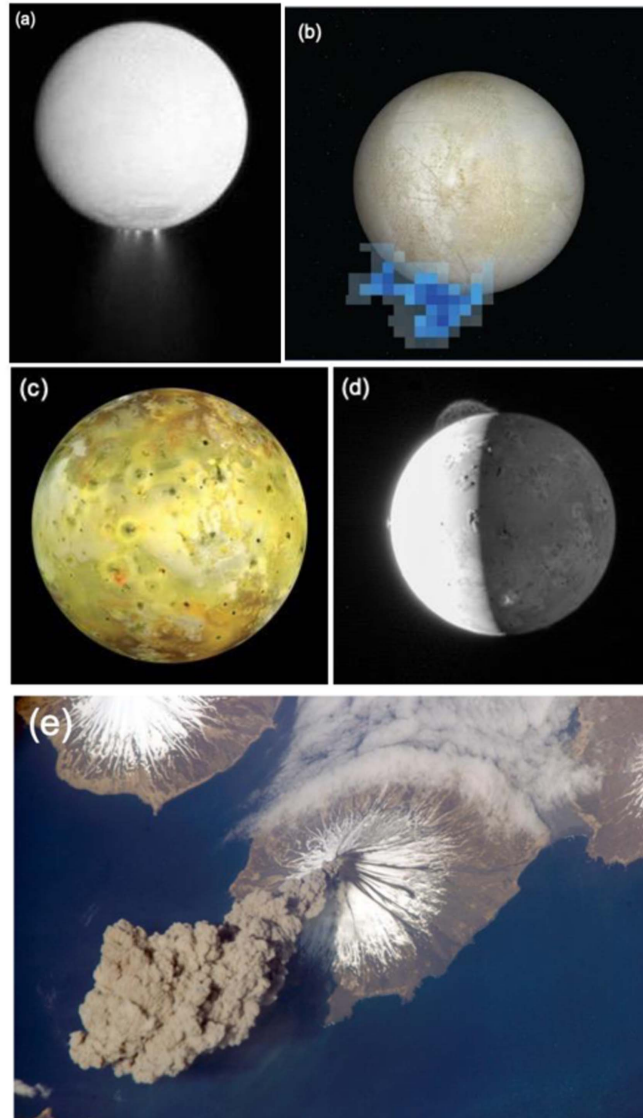


Figure 1. Explosive cryovolcanism, in the form of geyser-like plumes, has been detected on several of the icy moons in our solar system and volcanism is extensive on Jupiter's moon Io. Similarly, volcanic and cryovolcanic activity may be prevalent on the exoplanets in our study. (a) Plumes erupting at the south pole of Saturn's moon Enceladus, as imaged by the Cassini spacecraft. Enceladus' plumes extend up to 500 km above the surface and serve as a source of water vapor for Saturn's E-ring (Porco et al. 2006; Spencer et al. 2009). The material that is vented into space during Enceladus' cryovolcanic eruptions originates in a subsurface ocean (Postberg et al. 2009; Thomas et al. 2016). H_{Total} for Enceladus is 1.63×10^{10} W. (From NASA. Image stated to be in the public domain.) (b) The Hubble Space Telescope's STIS instrument detected plumes at the south pole of Jupiter's moon Europa. The pixelated blocks represent the locations where water vapor ejected during eruptions was detected spectroscopically. Europa's plumes may be up to 50–300 km tall (Roth et al. 2014b; Sparks et al. 2016, 2017) and may originate from pockets of water that are perched in its ice shell (Fagents et al. 2000). H_{Total} for Europa is 1.21×10^{12} W. (Image from ESA/Hubble.) LHS 1140 b and Trappist-1f may have explosive cryovolcanic eruptions in the form of geyser-like plumes similar to those on Europa and Enceladus (c) Galileo spacecraft image of Io, the most volcanically active body in our solar system ($H_{\text{Total}} = 1 \times 10^{14}$ W). The red, orange, black, brown and green patches on the surface represent numerous volcanic centers. In total, Io has >150 volcanic centers (Lopes et al. 2004; McEwen et al. 2004; Lopes & Williams 2015). (From NASA. Image stated to be in the public domain.) (d) The New Horizons spacecraft imaged several explosive volcanic eruptions on Io. Here, the 330 km tall plume from Io's Tvashtar volcano can be seen erupting at the top of the image (Spencer et al. 2007). Similarly, Super-Io exoplanets may have pervasive explosive eruptions at their surfaces. The large total internal heating rates for Super-Ios also indicate that they may have lava lakes and lava flows at their surfaces, as does Io. (From NASA. Image stated to be in the public domain.) (e) The explosive eruption of Mt. Cleveland in 2001 produced a massive plume (Dean et al. 2004). Similar plumes produced by larger explosive eruptions on supervolcanic planets could transport enough volcanic gases into their atmospheres for eruptions to be detected in transit spectra (Kaltenegger et al. 2010). Earth's H_{Total} is 4.7×10^{13} W, which is somewhat higher than H_{Total} for Venus (see below). Unlike Venus, however, Earth currently hosts an abundance of both effusive and explosive volcanic activity at the surface. Explosive volcanic activity manifests in a variety of ways on Earth (Carey & Bursik 2015; Cioni & Pistolesi 2015; Taddeucci et al. 2015). (From NASA. Image stated to be in the public domain.) See also Figure 2 and Tables 1 and 3.

(A color version of this figure is available in the online journal.)

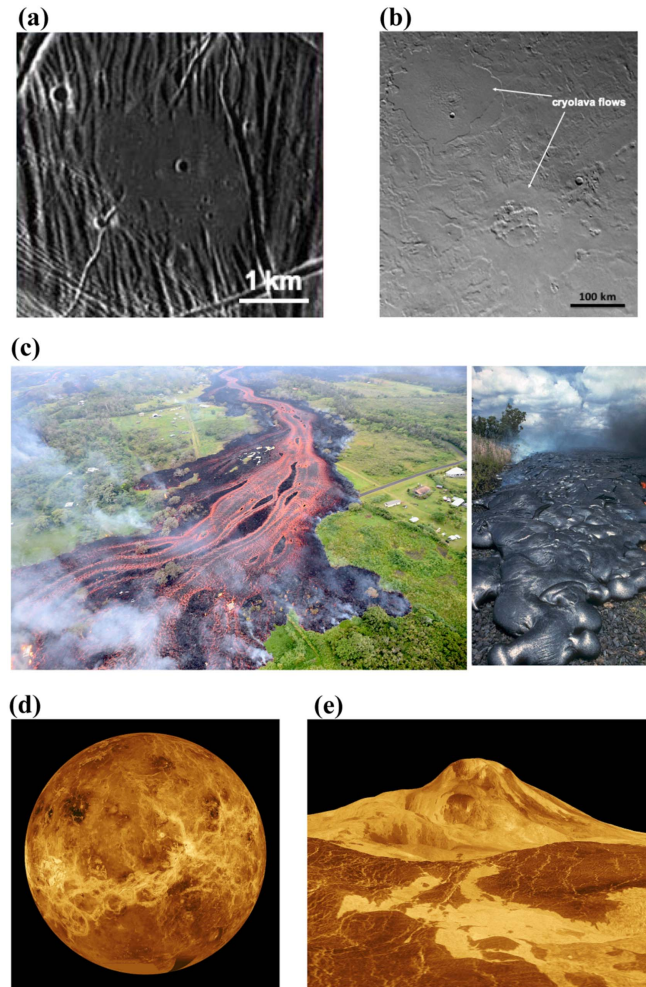


Figure 2. (a) This smooth, semi-circular feature on the surface of Jupiter's moon Europa ($H_{\text{Total}} = 1.21 \times 10^{12}$ W) is a cryolava flow that was emplaced during an effusive cryovolcanic eruption (Fagents 2003). (Adapted from original image from NASA. Image stated to be in the public domain.) (b) Cryolava flows on Neptune's moon Triton (Croft et al. 1995) ($H_{\text{Total}} = 1.37 \times 10^{11}$ W). Given their densities, effective temperatures, and the estimated magnitude of total internal heating, the surfaces of Trappist-1g and Trappist-1h may be covered in cryolava flows similar to those that have been imaged on Europa and Triton. (Adapted from original image from NASA. Image stated to be in the public domain.) (c) Effusive volcanism manifests in a variety of ways on Earth (Davies et al. 2010; Harris & Rowland 2015). Here we show terrestrial lava flows at two different scales and at two different temperatures. Left: massive lava flows issuing from Hawaii's Kilauea volcano. The bright red color indicates that this lava is still hot. Right: darker, chilled lava flowing from Kilauea. Like Earth, many of the exoplanets in our study may host both explosive and effusive volcanism at their surfaces. (From USGS. Image stated to be in the public domain.) (d) Magellan spacecraft radar image of the planet Venus ($H_{\text{Total}} = 2.9 \times 10^{13}$ W) showing many of the planet's volcanic centers and tectonic features (see Head et al. 1992). (From NASA. Image stated to be in the public domain.) (e) Magellan radar image of Venus' largest shield volcano, Maat Mons, with extensive lava flows in the foreground. These lava flows extend 100s of kilometers across the surface. While the vast majority of Venus' volcanoes are inactive, recent detections of fresh lava flows in the vicinity of Maat Mons suggest that Venus may still be volcanically active today (Shalygin et al. 2015). GJ 1132 b may boast extensive lava flows on its surface and magmatic activity in its subsurface, similar to Earth and Venus. (From NASA. Image stated to be in the public domain.) See also Figure 1 and Tables 1 and 3.

(A color version of this figure is available in the online journal.)

Cassini-spacecraft directly observed geyser-like plumes erupting from the south pole of Saturn's moon Enceladus (Porco et al. 2006; Spencer et al. 2009) (Figure 1). Effusive cryovolcanism, in which slurries of cryogenic fluids quiescently erupt, has been observed on both Europa (Fagents 2003; Miyamoto et al. 2005; Parro et al. 2016; Prockter et al. 2017; Quick et al. 2017b) and on Neptune's moon Triton (Croft et al. 1995) (Figure 2). We have utilized total internal heating rates, and the associated geological

activity on these planets and moons, as a baseline from which the expected rates of volcanic activity on terrestrial exoplanets can be inferred. Comparing the values of H_{Total} calculated for the planets in this study, with H_{Total} for the volcanically active planets and moons in our solar system (Table 1 and Figure 3) suggests that all of the exoplanets we considered are very volcanically active or very cryovolcanically active worlds. The close-in, high-eccentricity orbits of many of these planets ensure that they experience

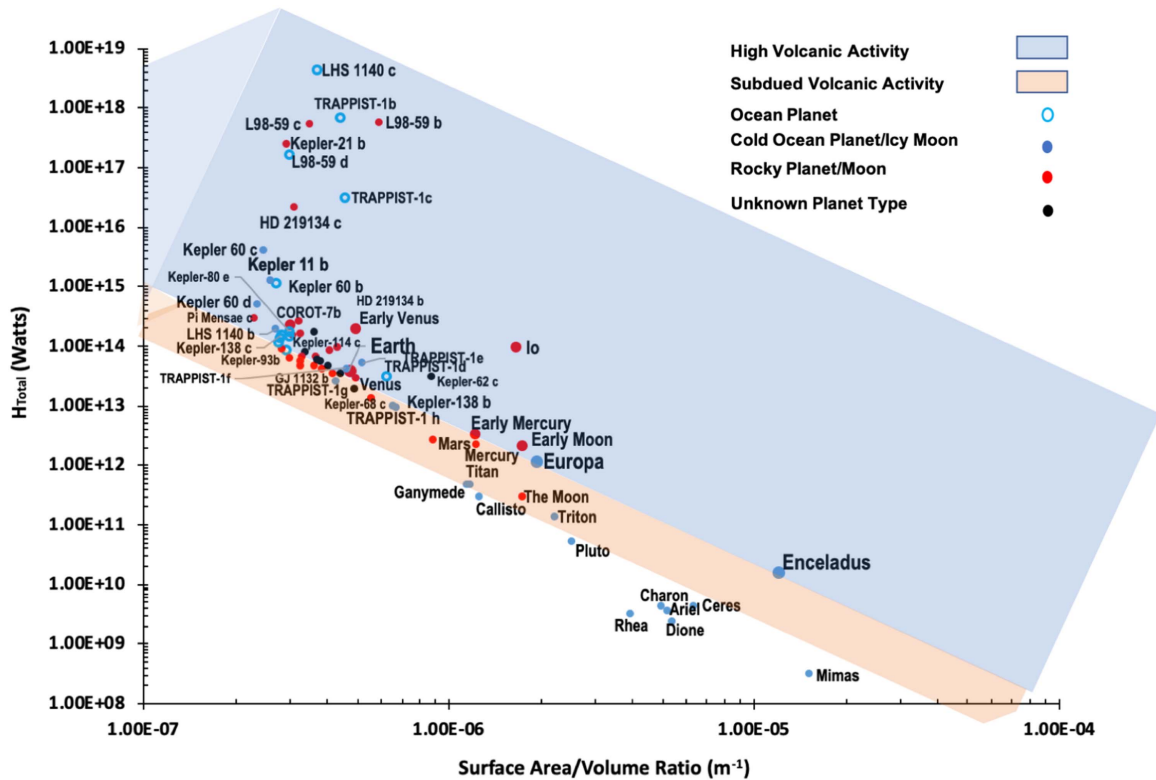


Figure 3. Based on rates of volcanic activity on Earth, and the rates of cryovolcanic activity on Europa and Enceladus, all exoplanets in our study are likely to be supervolcanic worlds. Planets within the blue shaded region are likely to have very high rates of volcanic or cryovolcanic activity, possibly replete with large explosive eruptions. Rocky planets are likely to be Super-Ios or Magma Ocean Worlds, and cold ocean planets are likely to display explosive cryovolcanic activity similar to that which occurs on Europa and Enceladus (Figure 1). We refer to all of these worlds as *High Volcanic Activity* planets. Planets within the orange shaded region will also be volcanically and cryovolcanically active, although their activity is expected to be more quiescent than that of their counterparts in the blue shaded region. Rocky exoplanets that lie in this region may be best categorized as Exo-Venus Planets. The volcanic or cryovolcanic activity on these bodies is likely to consist of effusive volcanic or cryovolcanic eruptions that produce lava or cryolava flows at their surfaces, along with internal convection and magmatism in their interiors. The activity on these worlds will be more subdued than the activity on their counterparts in the blue shaded region. We therefore refer to this activity as *Subdued Volcanic Activity*. Planetary bodies that plot below the orange shaded region may be geologically dead worlds. Based on this plot, the high rates of internal heating on cold, low-density planets such as LHS 1140b suggest that they may be Super-Europa/Super-Enceladus planets that exhibit explosive cryovolcanism similar to what has been observed on Europa and Enceladus (Figure 1). The slightly lower internal heating rates of Trappist-1g and Trappist-1h suggest that they may be similar to Neptune’s moon Triton, with internal convection and surfaces that are dominated by effusive cryovolcanism in the form of cryolava flows (Figure 2(b)) instead of explosive cryovolcanic eruptions. These planets may be best described as Super-Tritons. Our analysis suggests that CoRoT-7b may be a Magma Ocean World, based on its surface temperature and high internal heating rates.

(A color version of this figure is available in the online journal.)

significant amounts of tidal heating from their host stars. In addition, they are large enough to hold onto heat from the decay of radiogenic elements in their interiors for significant periods of time. This retention of heat ensures that the planets in our study will be very geologically active. In addition to being volcanically active, many of these worlds are likely to have pervasive tectonic activity at their surfaces (see Hurford et al. 2020) as they attempt to rid themselves of copious amounts of internal heat.

In an effort to further categorize the type of volcanic activity on the rocky exoplanets in our study, we will employ the naming conventions presented in Henning et al. (2018) to describe supervolcanic worlds (Table 3). For the purposes of this study, a supervolcanic world is any exoplanet with a total

internal heating rate that is comparable to Earth’s, where volcanic activity manifests as numerous explosive eruptions and/or lava flows at the surface, or as intense internal convection or magmatism. We consider *Super-Ios* to be rocky exoplanets where the amount of volcanic activity induced by internal heating is expected to exceed, or be comparable to, the amount of volcanic activity on Jupiter’s moon Io. This activity may manifest as numerous explosive or effusive eruptions at a planet’s surface. Regardless of their surface temperatures, H_{Total} for Super-Ios will be $\geq 10^{14}$ W. We envision that the surfaces of Super-Ios may resemble that of Io, which is dotted with more than 150 active volcanic centers (Figures 1(c) and (d)) (Lopes et al. 2004). Planets that are covered by global

magma oceans or that have at least one hemisphere that is covered by a magma ocean, will be denoted as *Magma Ocean Worlds* (Henning et al. 2018). Depending upon their SiO₂ content, melting temperatures for volcanic rocks range from ~973 to 1473 K, (Parfitt & Wilson 2008). Thus, $T_s = 973$ K can be considered to be a reasonable lower limit for the effective temperature of planets with molten surfaces. We therefore assume that any rocky planet in Table 1 with $T_s \geq 973$ K will have a completely molten surface and could therefore be a magma ocean world.

Henning et al. (2018) also mention *Exo-Venus Planets*, of which only a subset is expected to have high levels of volcanic activity. We therefore consider Exo-Venus planets to be planets that generally have low levels of volcanic activity that manifest as occasional explosive eruptions and lava flows. Exo-Venus planets may also have internal convection and magmatism. Venus' surface temperature is 700 K and its $H_{\text{Total}} = 3 \times 10^{13}$ W (Table 1). Exo-Venus planets may therefore have similar surface temperatures and similar total internal heating rates, on the order of a few 10^{13} W. Henning et al. (2018) also mention *lava worlds*, which they describe as planets with extensive lava lakes at their surfaces. As there are no planets or moons in our solar system that are considered to be lava worlds, it is not possible to specify ranges of T_s and H_{Total} for these worlds. For this reason, we do not consider lava worlds as an appropriate designation for the planets in our study and have not labeled any planets as such in Table 1. We have chosen to apply only the terms *Super-Io*, *Magma ocean world* and *Exo-Venus planet* to further characterize the rocky supervolcanic worlds in our study. Our categorizations for supervolcanic planets should be revisited should the characteristics of lava worlds, with respect to minimum surface temperature and characteristic internal heating rates, be further elucidated in the future.

3.1. Rocky Exoplanet Activity

In the context of this study we first consider 55 Cancri e, which observational analysis has suggested is a highly volcanic lava world that is completely melted on its day side (Demory et al. 2015, 2016), and Corot-7b, which has previously been characterized as a Super-Io (Barnes et al. 2010) and a lava-ocean planet (Léger et al. 2011). Although 55 Cancri e's exact composition is unknown its 6400 kg m^{-3} bulk density (Table 3) suggests that like Earth, it is primarily composed of rock and iron. Utilizing Equation (1) to calculate the tidal heating rate of 55 Cancri e returns $H_{\text{Tidal}} = 4.8 \times 10^{21}$ W (Table 1), while Equation (3) returns $M_{\text{mantle}} = 2.54 \times 10^{25}$ kg. If we assume that each planet's age is identical to the average estimated age of its host star, then the 10.2 Gyr age estimate for 55 Cancri (von Braun et al. 2011) can be utilized to obtain $\dot{h} = 4.49 \times 10^{-12} \text{ W kg}^{-1}$ for 55 Cancri e (Frank et al. 2014). Multiplying this value by M_{mantle} returns $H_{\text{Radiogenic}} = 1.14 \times 10^{14}$ (Table 1). In the case of Corot-7b, Equation (3)

returns $M_{\text{mantle}} = 1.4 \times 10^{25}$ kg. We have used the average estimated age of its host star, i.e., 1.32 Gyr (Barros et al. 2014), to obtain $\dot{h} = 1.59 \times 10^{-11} \text{ W kg}^{-1}$ (Frank et al. 2014). Multiplying this value by M_{mantle} as in Equation (4), returns $H_{\text{Radiogenic}} = 2.17 \times 10^{14}$ W for Corot-7b. If $e = 0$ for Corot-7b (Queloz et al. 2009; Barros et al. 2014; Stassun et al. 2017), $H_{\text{Tidal}} = 0$ and $H_{\text{Total}} = H_{\text{Radiogenic}} = 2.17 \times 10^{14}$ W (Table 1). H_{Total} for Io is between 1×10^{14} W and 2×10^{14} W (Veeder et al. 1994; Spencer et al. 2000). Since $H_{\text{Total}_{55\text{Cancri e}}} = 4.28 \times 10^7 H_{\text{Total}_{\text{Io}}}$, and $H_{\text{Total}_{\text{Corot-7b}}} = 2.17 H_{\text{Total}_{\text{Io}}}$, both of these planets are likely to be supervolcanic planets as described in Henning et al. (2018). As suggested in previous studies, 55 Cancri e likely exhibits extreme volcanism and may have a molten surface. Identical analyses of L98-59b & c (Kostov et al. 2019), assuming that L98-59 and its orbiting planets are at least 1 Gyr old, returns $H_{\text{Radiogenic}} = 3.33 \times 10^{13}$ W and 1.6×10^{14} W, respectively, with calculated H_{Tidal} and H_{Total} for each world being on the order of 10^{17} W. A simple comparison of H_{Total} for Io with $H_{\text{Radiogenic}}$ for the aforementioned planets (Table 1) makes it clear that even in the absence of tidal heating, 55 Cancri e, Corot-7b, and L98-59 b & c are all likely to exhibit extreme volcanism at their surfaces. Based on their total internal heating rates and their surface temperatures, which are well above 1000 K, 55 Cancri e and Corot-7b may be magma ocean worlds. The large H_{Total} for L98-59b & c suggests that their surfaces could be completely molten and that these planets could also be magma ocean worlds. However, as their surface temperatures are unknown (Table 1), we are unable to definitively characterize L98-59 b & c as such.

The results for H_{Total} presented in Table 1 can be employed to qualitatively assess the potential for volcanic activity on terrestrial exoplanets compared to the rates at which these processes occur on the planets and moons in our solar system. Owing to their large surface areas through which heat will escape, small planets will have much lower internal temperatures and will cool much faster than large planets (Stevenson 2003). This will ultimately result in the cessation of geological activity, including volcanism, at their surfaces. Thus in order to constrain the magnitude of volcanic activity occurring on the rest of the planets in our study, we have plotted H_{Total} as a function of surface area to volume ratio ($SA/V = 3/R_p$) for the planets and moons in our solar system and 52 terrestrial exoplanets, in Figure 3. Note that as a result of its large tidal heating rate, H_{Total} for 55 Cancri e is so large that it could not be plotted with the other worlds in Figure 3.

The blue shaded region in Figure 3 includes Earth, Enceladus, and Europa, all of which are replete with geological activity, including (cryo)volcanism and tectonics. Exoplanets that fall within this region of the plot are likely to exhibit rates of volcanic or cryovolcanic activity that are similar to, if not greater than, these bodies, and may contain internal oceans or magma layers. The exoplanets that plot far above Earth, Europa and Enceladus are likely to display pervasive volcanism at their

surfaces. Depending on where they plot, rates of volcanism on these exoplanets may be similar to rates of volcanism on Io, Early Venus, or Corot-7b. These exoplanets may be super-volcanic worlds, and volcanism on these bodies may one day be detectable in transit spectra (Kaltenegger et al. 2010; Quick et al. 2017a). Today, intense extrasolar volcanism may be detected in thermal emission observations (Demory et al. 2015) and in transmission spectra using high-resolution, ground-based spectrographs, provided that volcanic volatiles are lofted into their exospheres. Indeed Oza et al. (2019) report observational evidence of a volcanically-active exomoon orbiting the hot Jupiter WASP-49 b. These authors note that excesses in sodium observed in the planet's exosphere are indicative of an orbiting exomoon with Io-like volcanic activity. Although a detailed analysis that quantifies the detectability of extrasolar eruption signatures such as these will be the focus of a future effort, a basic atmospheric loss calculation for several of the rocky worlds in our study is provided in Section 4 (see below).

Planets that lie within the orange-shaded region of Figure 3 are likely to exhibit more subdued geological activity at their surfaces. Although these planets may not have extreme explosive volcanism like those in the blue-shaded region, effusive volcanism in the form of lava flows or cryolava flows may manifest on their surfaces, as may have recently been the case on the Moon (Garry et al. 2012; Braden et al. 2014; Qiao et al. 2017), Venus (Smrekar et al. 2010; Shalygin et al. 2015; Brossier et al. 2020; Filiberto et al. 2020) and Jupiter's icy moon Ganymede (Head et al. 1998; Schenk et al. 2001). Ongoing low-level volcanic activity in the form of magmatism, as has been suggested for Mars (Borg & Drake 2005; Sori & Bramson 2019), may also occur on these planets. These planets may also experience tectonic activity in the form of earthquakes like the Moon (Watters et al. 2019) and Mars (Giardini et al. 2020; Lognonné et al. 2020) (see Hurford et al. 2020 for a detailed discussion of tectonic activity on solid exoplanets). In addition, these planets may experience internal convection on regional scales, similar to Neptune's moon Triton (Schenk & Jackson 1993; Croft et al. 1995). Low-density planets may also contain global oceans in their interiors. The low-levels of volcanic activity on these bodies, combined with the possibility of intense internal convection and tectonic events, suggests that these worlds may be best classified as Exo-Venus planets. Based on its surface temperature and total internal heating rate, GJ 1132 b is likely to be an Exo-Venus planet. We hasten to add, however, that the current atmospheric state of GJ 1132 b is uncertain. At present, it could have a much thinner atmosphere than Venus, or may have completely lost its atmosphere due to atmospheric escape. Despite these uncertainties, we classify GJ 1132 b as an Exo-Venus planet,

and assume, based on its Venus-like total internal heating rate, that low levels of volcanic activity may occur at its surface. Although the total internal heating rates of planets such as Kepler 10 b and Kepler 101 c, both of which are on the order of a few 10^{13} W, suggest that they are Exo-Venus planets, their surface temperatures, which are 2130 K and 1412 K, respectively (Table 1), are warm enough for them to be magma ocean worlds. Accordingly, these planets have been labeled as magma ocean worlds in Table 1 despite their Venus-like heating rates.

Pluto, which sits just below the orange-shaded region in Figure 3, is known to have internal convection, albeit localized to only a few regions of the surface (McKinnon et al. 2016; Trowbridge et al. 2016), and may also contain a subsurface ocean (Hammond et al. 2016; Nimmo et al. 2016). It must be noted, however, that the maintenance of an ocean within Pluto may only be possible if the top of the ocean is capped by a layer of insulating clathrates (Kamata et al. 2019). Consideration of the incorporation of clathrates and other insulating materials into planetary interiors is beyond the scope of this work. Nevertheless, Pluto's internal state suggests that exoplanets with similar heating rates and surface area to volume ratios might also be able to maintain subsurface liquid reservoirs in special cases where substantial amounts of insulating materials have been incorporated into their interiors. Thus, the presence of low-eutectic contaminants such as ammonia, salts, and mineral acids may also promote the maintenance of oceans on small exoplanets. The incorporation of these species into the interiors of Trans-Neptunian Objects (TNOs) and the icy moons of the giant planets make it possible for oceans to exist within these bodies to the present day, particularly in cases where tidal heating is still in operation (Roberts & Nimmo 2008; Quick & Marsh 2015; Saxena et al. 2018). Similarly, the incorporation of clathrates and antifreezes may make it possible for bodies as small as Ceres to maintain small amounts of water until the present day (Neveu & Desch 2015; Fu et al. 2017; Castillo-Rogez et al. 2019; Quick et al. 2019).

Conversely, exoplanets that do not have insulating layers or antifreeze constituents in their interiors, have low internal heating rates, and large surface area to volume ratios, would quickly lose the little internal heat they have. Their present-day heating rates, $\leq 1 \times 10^{10}$ W, would be so low as to freeze all liquid in their interiors and render them geologically inactive today (Figure 3). Figure 3 illustrates that the majority of bodies that plot beneath the orange-shaded region have: small radii, on the order of hundreds of km, large surface area to volume ratios, and experience negligible tidal heating.

3.2. Extrasolar Ocean Worlds

Several of the terrestrial planets considered in our study may be more specifically described as ocean worlds or ocean

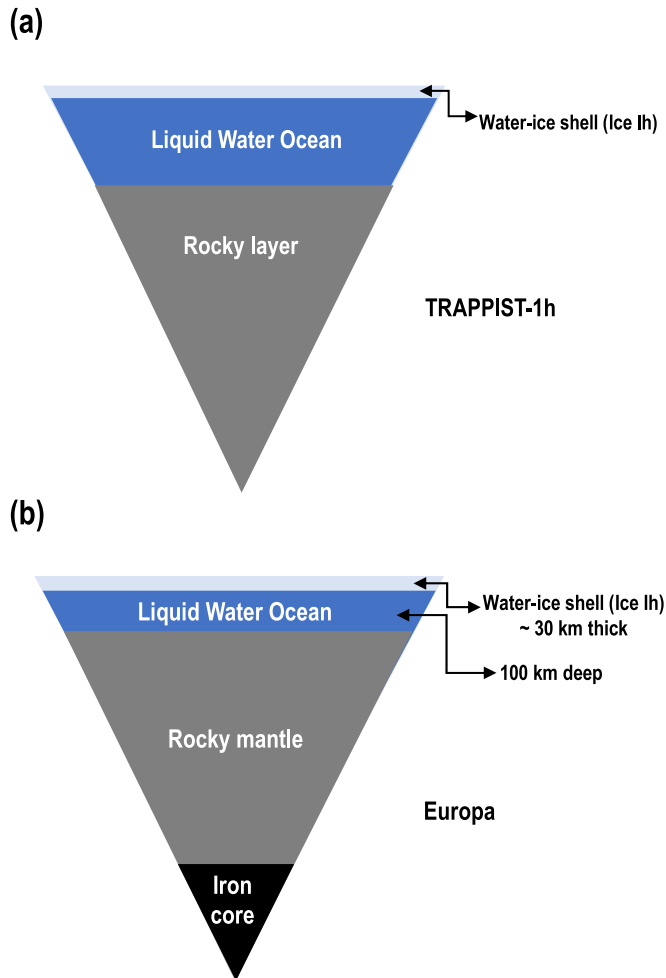


Figure 4. The internal structures of cold ocean planets may be similar to the internal structures of our solar system’s icy moons. According to models presented in Luger et al. (2017), Barr et al. (2018), and Dobos et al. (2019), the interior structure of Trappist-1h (a) could be similar to the interior structure of icy bodies like Jupiter’s moon Europa (b) (Schubert et al. 2009, and associated references in Table 1).

(A color version of this figure is available in the online journal.)

planets. Ocean planets are a class of low-density, terrestrial exoplanet with substantial water layers that may be common throughout the galaxy (Kuchner 2003; Léger et al. 2004; Ehrenreich & Cassan 2007; Sotin et al. 2007; Fu et al. 2010). These planets may exist in one of a variety of climactic states, including, ice-free, partially ice covered, and completely frozen (Budyko 1969; Sellers 1969; Tajika 2008). In the context of this study, planets that have conditions which are favorable to the maintenance of liquid water on their surfaces or in their interiors are assumed to be ocean planets. Conditions which may be favorable to the maintenance of liquid water include $T_{\text{EFF}} < 373$ K, or, in the case of high-gravity planets with potentially high surface pressures, i.e., surface pressures between 10^6 and 10^7 Pa (e.g., Kepler 138 c), T_{EFF} below the critical point (i.e., $T_{\text{EFF}} < 647$ K), and bulk densities below

5000 kg m^{-3} . The effective temperatures (Table 1) and proposed internal structures of Trappist-1 c & d (Barr et al. 2018) suggest that they could be ocean planets with surfaces that are covered in liquid water. This could be especially true of Trappist-1d (Dobos et al. 2019), as its low density is suggestive of a substantial fraction of volatiles (Table 1). We hasten to add, however, that owing to the extreme XUV emission of Trappist-1, it is possible that Trappist-1b-d may be currently experiencing a runaway greenhouse and/or that these planets have lost many oceans’ worth of water (Bolmont et al. 2017; Bourrier et al. 2017b). This type of extreme water loss could be an important signature that aids in the detectability and characterization of ocean planets. Nonetheless, H_{Total} for Trappist-1 c & d are 3×10^{16} W and 3×10^{13} W, respectively (Table 1). This indicates that they are likely to have extreme volcanism at their surfaces, or on their ocean floors, with Trappist-1 c being more volcanically active than Corot-7b (Figure 3), in agreement with the results of previous analyses (Dobos et al. 2019).

We refer to exoplanets with ice-covered surfaces that overlie internal oceans (Kuchner 2003; Ehrenreich et al. 2006; Ehrenreich & Cassan 2007; Tajika 2008; Yang et al. 2017) as *cold ocean planets*. The internal structures of cold ocean planets may resemble the internal structures of our solar system’s icy moons (Figure 4) (Ehrenreich et al. 2006; Sotin et al. 2007; Vance et al. 2007, 2015; Fu et al. 2010; Henning & Hurford 2014; Noack et al. 2016; Luger et al. 2017; Barr et al. 2018), and they may exhibit similar geological activity at their surfaces, including ice tectonics (Fu et al. 2010; Levi et al. 2014) and cryovolcanism (Levi et al. 2013; Quick et al. 2017a; Barr et al. 2018; Quick & Roberge 2018). In the absence of an atmosphere, Earth’s effective temperature of 255 K (Sagan & Mullen 1972) allows for the maintenance of liquid water at the surface. We therefore assume that cold ocean planets have $T_{\text{EFF}} < 255$ K. Several of the planets plotted in Figure 3 have $T_{\text{EFF}} < 255$ K, and/or densities that are $\leq 3500 \text{ kg m}^{-3}$ (Table 1), commensurate with density values of our solar system’s icy moons (Jacobson et al. 1992; Anderson et al. 1997; Hussmann et al. 2006). Based on their surface temperatures and bulk densities, we have designated these exoplanets as cold ocean planets.

The effective temperatures, densities, and total internal heating rates of Kepler 138-b & d, Trappist-1e, f, g & h, Kepler 60-c & d and Kepler 11 b suggest that these planets could be cold ocean planets that have persistent cryovolcanic activity at their surfaces (Table 1 and Figure 3). Although LHS 1140 b’s high-density is indicative of an iron-rich terrestrial planet (Dittmann et al. 2017b; Ment et al. 2019), its 235 K surface temperature (Ment et al. 2019) suggests that any water on its surface would be in a frozen state. Further, its estimated total internal heating rate of almost 2×10^{14} W may be high enough for it to maintain an internal ocean and cryovolcanic eruptions at its surface. While cryovolcanic activity on Kepler 138-b and

Trappist 1-g & h may be more subdued than what has been observed on Enceladus and Europa (Figure 1), their positions in Figure 3 suggest that they may undergo periodic resurfacing by cryolava flows and/or that they may experience periodic outgassing of volatiles as is the case on planet Venus (e.g., see Bondarenko et al. 2010; Smrekar et al. 2010; Shalygin et al. 2015). Thus, cryolava flows on the surfaces of these planets may be similar to what has been observed in the walled plains units of Neptune’s moon Triton and in certain regions of Europa (Figures 2(a) and (b)), albeit more widespread. Explosive cryovolcanism, similar to what has been observed on Enceladus and Europa (Figure 1), may occur at comparable magnitudes on Kepler 138 d, Trappist-1f and LHS 1140 b.

According to Figure 3, rates of cryovolcanism on Trappist-1e and Kepler 60 d may be similar to rates of volcanism on Jupiter’s moon Io, while Kepler 11 b and 60c are likely to exhibit extreme cryovolcanism. Internal heating rates for these planets, on the order of 10^{15} W (Table 1 and Figure 3), suggest that the rates of cryovolcanism at their surfaces could exceed the rate of silicate volcanism that occurs on Corot-7b by an order of magnitude. Based on their internal heating rates and surface area to volume ratios compared to the planets and moons in our solar system (Figure 1), all of the aforementioned exoplanets may contain extensive reservoirs of liquid water, possibly in the form of global oceans beneath layers of surface ice.

We have further characterized cold ocean planets as Super-Europa/Super-Enceladus planets and Super-Tritons (Table 3). We envision that the total internal heating rates of Super-Europa/Super-Enceladus planets are large enough for them to have explosive cryovolcanic eruptions in the form of geyser-like plumes (Figures 1(a) and (b)), effusive cryovolcanism that manifests as cryolava flows on their surfaces (Figures 2(a) and (b)), and internal convection and cryomagmatism. Conversely, cryovolcanism on Super-Tritons will be dominated by effusive cryovolcanism in the form of cryolava flows, although these planets may also have intense internal convection and cryomagmatism. Both types of cold ocean planets are likely to have internal oceans. We conclude that LHS 1140 b, Trappist-1e, and Trappist-1f may be Super-Europa/Super-Enceladus planets, while Trappist-1g and Trappist-1h may be Super-Tritons (Tables 1 and 3). As is the case for Europa (Crawford & Stevenson 1988; Fagents 2003) and Enceladus (Manga & Wang 2007; Běhounková et al. 2015), cryovolcanic eruptions on these worlds may provide a pathway by which ocean water, or the contents of discrete water pockets within their ice shells, reaches the surface. It must be noted that in the case of Trappist-1f, g, & h, $H_{\text{Radiogenic}}$ is greater than, or equal to, H_{Tidal} (Table 1). Hence, even if these planets are too far away from their host star to experience substantial tidal heating (Dobos et al. 2019), they are still likely to be geologically active and able to maintain subsurface oceans.

The densities and/or effective temperatures of Trappist-1b, Kepler 93 b, Kepler 138 c, Kepler 114 c, Kepler 80 e, LHS 1140c, Pi Mensae c, and L98-59 d are such that they could also be ocean planets or cold ocean planets. If surface pressures on these planets are high enough, liquid water could be maintained at their surfaces at the critical point, or they could contain high pressure ices. Although these planets have been plotted as ocean planets in Figure 3, we label them as candidate ocean planets in Table 1. With the exception of Kepler 114 c, for which we were unable to obtain H_{Total} due to the unknown age of its host star and its unknown eccentricity, estimated internal heating rates for all of these planets suggest that they are all likely to be (cryo) volcanically active (Figure 3). Notably, Pi Mensae c and L98-59 d likely receive enough internal heating from radiogenic sources alone to be as volcanically active as Io (Table 1 and Figure 3), while LHS 1140c may receive enough internal heating from radiogenic sources alone to be as geologically active as Earth. Ment et al. (2019) report an eccentricity less than 0.31 for LHS 1140c. Using 0.31 as an upper bound for eccentricity in Equation (1) results in tidal and total internal heating rates for this planet that are several orders of magnitude greater than the tidal and total internal heating rates of Corot-7 b (Table 1 and Figure 3). Such high internal heating rates would suggest that LHS 1140 c is a magma ocean world instead of a candidate ocean world. However, owing to uncertainties in e (Ment et al. 2019) the estimated H_{Total} for this planet represents a maximum value that may change once e is better constrained. Bearing this in mind, we contend that LHS 1140c could be an ocean world that contains exotic forms of ice on its surface or within its interior. Due to its high T_{EFF} and low density, Pi Mensae c could also contain exotic forms of ice.

Europa and Ganymede’s mantles comprise 69% and 40% of their total volumes, respectively. This information can be utilized to determine $H_{\text{Radiogenic}}$ for ocean planets when their internal structures are similar to the internal structures of these icy moons (Table 2). For these cases, the procedures outlined in Equations (2)–(4) can be applied if Equation (2) is replaced by $V_{\text{mantle}} = 0.69V_P$ and $V_{\text{mantle}} = 0.4V_P$ for planets with mantle volumes that are similar to Europa and Ganymede, respectively (see Appendix). It is clear from Table 2 that assuming mantle volumes similar to Europa and Ganymede returns radiogenic heating rates and total internal heating rates that are generally of the same order of magnitude as when an Earth-like mantle volume was applied in Section 2. As before, H_{Total} obtained from these calculations suggest that all of the exoplanets considered here are likely to be cryovolcanically active. Thus, the results discussed in Sections 3.1 and 3.2 remain unchanged.

Similar to the case for volcanism on rocky exoplanets, water vapor and other volatiles that are lofted into the exospheres of cold ocean planets during cryovolcanic eruptions could be detected in transmission spectra using high-resolution ground-based telescopes. The presence of copious amounts of water

Table 2
Exoplanet Heating Rates for Various Internal Structures [1 W = 10^7 erg s $^{-1}$]

World	R_P (R_{\oplus})	M_P (M_{\oplus})	$H_{\text{Radiogenic}}$ for Europa-like Structure (W)	$H_{\text{Radiogenic}}$ for Ganymede-like Structure (W)	H_{Tidal} (W)	H_{Total} for Europa-like Internal Structure (W)	H_{Total} for Ganymede-like Internal Structure (W)	Type
^a HD 219134 f	1.31	unknown	2.52×10^{13}	1.46×10^{13}	1.42×10^{14}	1.67×10^{14}	1.57×10^{14}	unknown
Kepler 11 b	1.8	1.9	7.7×10^{13}	4.5×10^{13}	^b 1.12×10^{15}	1.2×10^{15}	1.16×10^{15}	cold ocean planet
Kepler 60 b	1.68	4.2	8.53×10^{13}	4.94×10^{13}	9.4×10^{14}	1.03×10^{15}	9.89×10^{14}	ocean planet
Kepler 60 c	1.9	3.85	1.23×10^{14}	7.15×10^{13}	3.81×10^{15}	3.93×10^{15}	3.88×10^{15}	cold ocean planet
Kepler 60 d	1.99	4.16	1.42×10^{14}	8.22×10^{13}	3.03×10^{14}	4.45×10^{14}	3.85×10^{14}	cold ocean planet
Kepler 62 c	0.54	unknown	2.33×10^{12}	1.35×10^{12}	TBD: e unknown	2.33×10^{12}	1.35×10^{12}	unknown
Kepler 68 c	0.96	2.04	1.4×10^{13}	8.1×10^{12}	0 ($e = 0$)	1.4×10^{13}	8.1×10^{12}	unknown
Kepler 80 e	1.6	4.1	1.36×10^{14}	7.89×10^{13}	TBD: e unknown	1.36×10^{14}	7.89×10^{13}	candidate ocean planet
Kepler 93 b	1.6	3.2	6.28×10^{13}	3.64×10^{13}	0 ($e = 0$)	6.28×10^{13}	3.64×10^{13}	candidate ocean planet
Kepler 114 c	1.6	2.8	1.13×10^{14}	6.53×10^{13}	TBD: e unknown	1.13×10^{14}	6.53×10^{13}	candidate ocean planet
Kepler 138 b	0.7	0.19	6.5×10^{12}	3.77×10^{12}	5.33×10^{11}	7.04×10^{12}	4.3×10^{12}	cold ocean planet
Kepler 138 c	1.7	5.2	9.32×10^{13}	5.4×10^{13}	3.2×10^{13}	1.25×10^{14}	8.6×10^{13}	candidate ocean planet
Kepler 138 d	1.7	1.2	9.32×10^{13}	5.4×10^{13}	1.5×10^{13}	1.08×10^{14}	6.9×10^{13}	ocean planet
Kepler 186 b	1.07	unknown	2.58×10^{13}	1.5×10^{13}	TBD: e unknown	2.58×10^{13}	1.5×10^{13}	unknown
Kepler 186 c	1.25	unknown	4.12×10^{13}	2.39×10^{13}	TBD: e unknown	4.12×10^{13}	2.39×10^{13}	unknown
Kepler 186 d	1.4	unknown	5.79×10^{13}	3.36×10^{13}	TBD: e unknown	5.79×10^{13}	3.36×10^{13}	unknown
Kepler 186 e	1.27	unknown	4.32×10^{13}	2.51×10^{13}	TBD: e unknown	4.32×10^{13}	2.51×10^{13}	unknown
Kepler 186 f	1.2	unknown	3.65×10^{13}	2.11×10^{13}	1.1×10^9	3.65×10^{13}	2.11×10^{13}	unknown
Kepler 414 b	1.7	3.5	8.43×10^{13}	4.89×10^{13}	TBD: e unknown	8.43×10^{13}	4.89×10^{13}	ocean planet
L 98-59 d	1.57	3.4	1.81×10^{14}	1.05×10^{14}	1.68×10^{17}	1.68×10^{17}	1.68×10^{17}	candidate ocean planet
LHS 1140 b	1.73	6.98	9.43×10^{13}	5.47×10^{13}	^c 6.15×10^{13}	1.56×10^{14}	1.16×10^{14}	cold ocean planet
LHS 1140c	1.3	1.81	4×10^{13}	2.32×10^{13}	^c 4.38×10^{18}	4.38×10^{18}	4.38×10^{18}	candidate ocean planet
Trappist-1 b	1.07	0.85	1.68×10^{13}	9.72×10^{12}	7.02×10^{17}	7.02×10^{17}	7.02×10^{17}	candidate ocean planet
Trappist-1 c	1.04	1.38	1.54×10^{13}	8.92×10^{12}	3.13×10^{16}	3.13×10^{16}	3.13×10^{16}	ocean planet
Trappist-1 d	0.76	0.41	6.01×10^{12}	3.48×10^{12}	2.3×10^{13}	2.9×10^{13}	2.65×10^{13}	ocean planet
Trappist-1 e	0.9	0.64	9.97×10^{12}	5.78×10^{12}	3.84×10^{13}	4.84×10^{13}	4.42×10^{13}	cold ocean planet
Trappist-1 f	1.03	0.67	1.49×10^{13}	8.67×10^{12}	2.31×10^{13}	3.8×10^{13}	3.18×10^{13}	cold ocean planet

Table 2
(Continued)

World	$R_p (R_\oplus)$	$M_p (M_\oplus)$	$H_{\text{Radiogenic}}$ for Europa-like Structure (W)	$H_{\text{Radiogenic}}$ for Ganymede-like Structure (W)	H_{Tidal} (W)	H_{Total} for Europa-like Internal Structure (W)	H_{Total} for Ganymede-like Internal Structure (W)	Type
Trappist-1 g	1.11	1.34	1.87×10^{13}	1.08×10^{13}	5.77×10^{11}	1.93×10^{13}	1.14×10^{13}	cold ocean planet
Trappist-1 h	0.72	0.086	5.11×10^{12}	2.96×10^{12}	3.03×10^{12}	8.14×10^{12}	5.99×10^{12}	cold ocean planet

Notes. Heating rates for Ocean Planets and planets of unknown type (see Table 1) considering internal structures similar to Europa ($V_{\text{mantle}} = 0.69 V_p$) and Ganymede ($V_{\text{mantle}} = 0.4V_p$) instead of Earth.

^a Smallest possible value of R_p from Gillon et al. (2017a).

^b In order to obtain a conservative tidal heating rate, we have used the eccentricity value reported in Borsato et al. (2014) ($e = 0.026$) in Equation (1).

^c Eccentricity is poorly constrained; maximum eccentricity values substituted into (1). H_{Tidal} is preliminary.

vapor and its constituent atoms in the exospheres of low-mass exoplanets with low effective temperatures and densities could therefore serve to confirm their status as cryovolcanically-active cold ocean planets.

We note that utilizing Equation (1) to determine H_{Total} for Io and Enceladus where Jupiter and Saturn serve as the primaries from which tidal heating is sourced, returns total internal heating rates of 2×10^{13} W and 3.2×10^8 W, respectively, which are 1–2 orders of magnitude less than their actual values of 1×10^{14} W, and 1.6×10^{10} W, respectively (Veeder et al. 1994; Spencer et al. 2000; Schubert et al. 2004; Howett et al. 2011). This discrepancy suggests that substituting $k_2 = 0.3$ and $Q = 100$ in Equation (1) returns conservative values for exoplanet tidal heating rates, and by extension, for the magnitude of geological activity that may be occurring at the surfaces of the planets we have considered. In order to ensure maximum accuracy when constraining the amount of volcanic activity on the exoplanets listed in Table 1, specific k_2 and Q values must be determined for each planet. This would require a new modeling approach that would allow us to constrain the relative amounts of ice, metal, and rock likely to be present in each of the exoplanets considered. This approach was employed in Barr et al. (2018) and could be utilized to confirm the terrestrial status of the largest planets in our study, including, Kepler 60 c & d, LHS 1140 b, Kepler 138 c, and Pi Mensae c. All of these planets have radii greater than $1.6R_{\oplus}$, which could be indicative of a sub-Neptune-like composition (Rogers 2015; Jin & Mordasini 2018). Such an approach, which would also include an in-depth analysis of the internal structures of the cold ocean planets identified in this study, will be the focus of a forthcoming manuscript. Indeed, we have assumed that all of the cold ocean planets in our study are *Super-Europa* or *Super-Enceladus planets*, consisting of thin external ice shells overlying oceans that are in direct contact with a rocky mantle. Such worlds may also have a small iron core (Figure 4). However, the cold ocean planets listed in Tables 1 and 3 could also be *Super-Ganymedes*. In that case, these worlds would have oceans that are sandwiched between very thick (\geq approximately 100 km thick) external ice shells and sub-ocean layers of high-pressure ice, beneath which rocky mantles and iron cores lie (see Anderson et al. 1996; Vance et al. 2014, 2015). Owing to this internal configuration in which oceans would not be in direct contact with silicate mantles, cryovolcanism on Super-Ganymedes would occur sporadically and would likely manifest as effusive cryovolcanism in the form of occasional cryolava flows at their surfaces (Kay & Head 1999; Schenk et al. 2001; Showman et al. 2004) Both Europa-like and Ganymede-like internal structures are permissible for cold ocean planets (Luger et al. 2017; Barr et al. 2018) and should be explored further in the future.

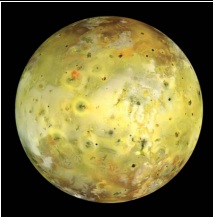

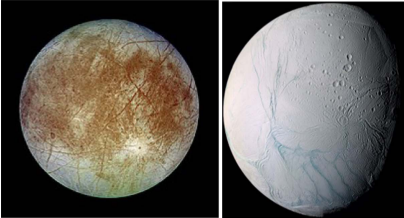

4. Conclusions

We have not considered additional exoplanet heating sources, such as those that might be contributed by stellar radiation (see Barr et al. 2018), or dynamical planet–planet or planet-moon interactions within exoplanetary systems in our analyses. However, contributions from stellar radiation may be significant (Guenther & Kislyakova 2020). We have also neglected to consider cases in which the dynamical histories and internal structures of planetary bodies could preclude substantial internal heating. This is the case for Saturn’s moon Mimas. Although Mimas is known to be a geologically dead world (Rhoden et al. 2017; Kirchoff et al. 2018), utilization of Equation (1) returns a tidal heating rate that suggests that the small moon should be more geologically active than Enceladus. Neveu & Rhoden (2019) suggest that the absence of current geological activity on Mimas may be due to a loss of radiogenic heating early in its evolution. The authors assert that loss of radiogenic heating precluded Mimas from having a dissipative interior. However, such considerations for Earth-like exoplanets are beyond the scope of this work.

Additionally, as the planets in our study have been categorized as Super-Ios, Magma Ocean Worlds, Exo-Venus Planets, Super-Europa/Super-Enceladus planets and Super-Tritons based on their surface temperatures and total internal heating rates, we have made no attempt to further categorize planets for which T_s is unknown, planets of “unknown” type (i.e., planets for which there is not enough information to determine whether they are rocky planets, ocean planets or cold ocean planets in Table 1) or ocean planets, for which it is unknown whether the bulk of their volcanic activity would occur on their ocean floors, or at their surfaces.

Finally, our analysis has not included the effects of induction heating, which could serve as an additional heat source for driving volcanic activity on close-in exoplanets (Garraffo et al. 2017; Kislyakova et al. 2018; Guenther & Kislyakova 2020). Recent studies focusing on induction heating of the Trappist-1 planets have revealed that the amount of heating imparted by this process would be at least an order of magnitude less than the amount of heating that these planets would experience due to tidal interactions with their host stars (Garraffo et al. 2017; Kislyakova et al. 2017). In the case of Trappist-1b, the amount of heat imparted by tidal interactions, 7×10^{17} W (Table 1), is greater than that experienced due to induction heating, 5×10^{12} W (Kislyakova et al. 2017), by 5 orders of magnitude. This is in agreement with past work which suggested that tidal heating surpasses induction heating in the Trappist-1 system (Luger et al. 2017). Guenther & Kislyakova (2020) explored prospects for volcanism on HD3167 b assuming that volcanic activity would be driven by induction heating or melting of the surface due to intense stellar radiation. The amount of induction heating these authors estimate for HD3167 b ranges from 10^{12} to 10^{15} W, with the latter value

Table 3
Supervolcanic Exoplanet Categories [$1 W = 10^7 \text{ erg s}^{-1}$] This Table includes Descriptions and Examples of each Type of Supervolcanic World for which an Analog Exists in our Solar System

Category	Solar System Analog	Potential Examples
Super-Io	 <p>Io $H_{Total} = 1 \times 10^{14} W$ <i>Lopes et al. [2004]; McEwen et al. [2004]; Lopes and Williams [2015]</i></p>	HD 219134 c, Kepler 80 d
Exo-Venus Planet	 <p>Venus $H_{Total} = 2.91 \times 10^{13} W$ <i>Head et al. [1992]; Shalygin et al. [2015]; Filiberto et al. [2020]</i></p>	GJ 1132b
Super-Europa/Super-Enceladus Planets	 <p>Europa (left) $H_{Total} = 1.21 \times 10^{12} W$ <i>Fagents et al. [2000]; Fagents, [2003]; Roth et al. [2014a]; Geissler et al. [2015]; Sparks et al. [2016; 2017]</i> Enceladus (right) $H_{Total} = 1.63 \times 10^{10} W$ <i>Porco et al. [2006]; Spencer et al. [2009]; Geissler et al. [2015]</i></p>	LHS 1140 b, Trappist-1d, Trappist-1e, Trappist-1f
Super-Triton	 <p>Triton $H_{Total} = 1.37 \times 10^{11} W$ <i>Croft et al. [1995]; Geissler et al. [2015]</i></p>	Trappist-1g, Trappist-1h

Note. Magma Ocean Worlds (e.g., 55 Cancri e, Corot-7b) have not been included here, as no analogs for these types of planets exist in our solar system. See Figures 1 and 2 for detailed descriptions of the ways in which volcanism/cryovolcanism may manifest on these worlds.

being representative of the estimated amount of heating imparted by induction when the planet was young. Induction heating rates of 1.8×10^{12} – 4.5×10^{13} W, corresponding to stellar dipole fields on the order of 10^{-4} T (1–5 G), are much less than the $\sim 10^{14}$ W of radiogenic heating that this planet experiences today (Table 1). Moreover, while induction heating may have played a significant role in driving volcanic activity on HD 3167 b when HD 3167 was young (Guenther & Kislyakova 2020), the system’s average estimated age of 7.8 Gyr (Christiansen et al. 2017) suggests that induction heating is much less of a driver for volcanic activity on this planet than radiogenic heating is today. Our results suggest that even without accounting for additional heating from its host star, HD 3167 b can be classified as a supervolcanic planet owing to its present-day radiogenic heating rate alone (Table 1 and Figure 3). These results are in agreement with previous assessments by Guenther & Kislyakova (2020) that HD3167 b has a molten surface and is an ideal place to search for an exosphere. Indeed, HD3167 b’s high surface temperature and H_{Total} suggest that this planet is a magma ocean world (Table 1). Since $H_{\text{Total,HD 3167b}} \sim H_{\text{Total,Io}}$, we argue that in addition to intense heating by its host star, that widespread magmatism induced by the planet’s endogenic heating plays a significant role in creating HD 3167 b’s molten surface.

It must be noted that variations in exoplanet eccentricity may affect the timing and strength of volcanism at the surfaces of the planets plotted in Figure 3. Recent studies have attempted to predict the timing and strength of volcanism at Io’s surface based on variations in its eccentricity as it orbits Jupiter. Similar to the case of the geyser-like plumes on Enceladus (Figure 1(a)) (Hedman et al. 2013), observations of the Ionian volcano Loki Patera, which is responsible for $\geq 10\%$ of Io’s heat flow (Veeder et al. 1994), suggest that volcanic activity on the Jovian moon may vary with its orbital phase. Io experiences the greatest amount of tidal heating and volcanic activity at apoiove, when its average eccentricity is the highest (de Kleer et al. 2019a, 2019b). In addition, periodicities in tidal forcing and eruption strength are likely to exist on Io, with recent eruptions occurring on 440–475 day periods (de Kleer et al. 2019a; Rathbun et al. 2019). If volcanism on tidally heated exoplanets operates similarly to volcanism on the tidally heated bodies in our solar system, this would suggest that extrasolar volcanism may also be periodic, and that tidally locked planets may experience the greatest amount of internal heating and elevated volcanism at apoapsis. The results of the aforementioned studies could then be used as a baseline to predict the time during their orbits in which volcanic eruptions are likely to be the strongest, and hence most detectable, on solid exoplanets. We also hasten to add that while explosive cryovolcanic activity on Enceladus is abundant and continuous (Spencer et al. 2009; Postberg et al. 2018a), spectroscopic detections using ground-based telescopes (Roth et al. 2014a, 2014b; Paganini et al. 2019), modeling (Fagents et al. 2000;

Quick et al. 2013; Rhoden et al. 2015; Quick & Hedman 2020), and previous searches for plumes in the Galileo data set (Phillips et al. 2000), all suggest that explosive cryovolcanism on Europa may be small-scale and/or sporadic in nature. Thus, future observational searches for explosive cryovolcanic activity on cold ocean planets should be undertaken with the knowledge that activity on these bodies could be transient in nature and possibly difficult to detect. Accordingly, searches for variability at transiting exoplanets would be useful.

Io has a history of extreme volatile loss, much of which includes the loss of volcanically produced SO_2 , S, and O to its exosphere via interactions with solar energetic particles (McGrath et al. 2004 and references therein). Thus, comparisons of the magnitudes of atmospheric loss between Io and the rocky exoplanets we have considered could further confirm their categorization as Super-Ios, magma ocean worlds, or Exo-Venus planets, while simultaneously revealing the state of their atmospheres. We have therefore employed methods for observing an exo-Io (see Oza et al. 2019) to perform a basic atmospheric loss calculation for several of the rocky planets listed in Table 1, assuming that SO_2 is their primary atmospheric constituent and volcanic volatile, as on Io. This basic calculation allows us to estimate the magnitude of energy-limited escape induced by incoming XUV radiation, and the associated line of sight (LOS) column densities of SO_2 for these worlds (Table 4). Incident XUV fluxes for each planet, F_{XUV} , as a function of system age and host star spectral type, were obtained using the methods of Lammer et al. (2009), while the magnitude of energy-limited escape was calculated using Equation (9) of Oza et al. (2019), assuming an efficiency factor for SO_2 , η_{XUV} , of 0.35, a mass fraction of SO_2 , x_i , of ~ 1 , as is the case for Io’s atmosphere (Lellouch et al. 1992, 1996), and assuming that $R_a \cong R_p$ so that U_s is representative of the gravitational binding energy of SO_2 at an adsorption altitude R_p (see Johnson et al. 2015). Equation (13) of Oza et al. (2019) was then employed to obtain the disk-averaged, line of sight column density of SO_2 , $\langle N \rangle$, as a function of host star radius and the SO_2 photoionization time, τ_i , of each exoplanet. The results of these calculations represent the evaporating column density of SO_2 in transmission spectroscopy (Table 4).

The photoionization time of SO_2 on Io, τ_{Io} , is approximately 20 days (1.7×10^6 s) (Kumar 1979). As the photon flux from the host star is proportional to $1/a_p^2$, where a_p is the planet’s semimajor axis, the photoionization time of SO_2 on each exoplanet may be obtained by scaling according to Io’s SO_2 photoionization lifetime, i.e., $\tau_i = \tau_{\text{Io}} \times (a_p/a_{\text{Io}})^2 = 1.7 \times 10^6 \text{ s} \times (a_p/a_{\text{Io}})^2$, where a_p for each exoplanet is listed in Table 4. Table 19.1 in McGrath et al. (2004) reports line of sight column densities of SO_2 at Io on the order of 10^{18} – 10^{21} molecules m^{-2} , while Lellouch et al. (2015) report column densities ranging from 3×10^{20} to 1.5×10^{21} molecules m^{-2} for SO_2 on Io. According to our calculations, line of sight column densities of SO_2 on the exoplanets listed in Table 4 would be ~ 2 to 4 orders of magnitude

Table 4Column Densities and Outgassing Rates for Rocky Supervolcanic Planets Assuming that their Atmospheres/exospheres are Dominated by SO₂ and/or that SO₂ is their Primary Volcanic Volatile, as is the case for Jupiter's Moon Io

Planet	Stellar Spectral Type	a_P (au)	Line of Sight Column Density of SO ₂ (Evaporative Column Density) $\langle N \rangle$ (molecules m ⁻²)	SO ₂ Mass Loss Rate (kg s ⁻¹)	Volcanic Column Density of SO ₂ , NO (molecules m ⁻²)	Tidally-driven Volcanic Outgassing Rate of SO ₂ (kg s ⁻¹)
Kepler 78 b	G	0.01	2.0×10^{16}	2.9×10^8	^a ...	^a ...
55 Cancri e	G	0.015	3.2×10^{14}	3.3×10^6	4.9×10^{25}	3.0×10^{14}
GJ 1132 b	M	0.0153	6.5×10^{15}	3.2×10^6	^a ...	^a ...
Corot-7b	G	0.017	9.9×10^{15}	6.1×10^7	^b 0	^b 0
Kepler 10 b	G	0.0172	1.8×10^{14}	1.8×10^6	^a ...	^a ...
HD 3167 b	K	0.0186	2.6×10^{14}	1.5×10^6	^b 0	^b 0
L 98-59 b	M	0.0233	3.0×10^{16}	1.4×10^7	^c ...	4.0×10^{10}
L 98-59 c	M	0.0324	3.0×10^{16}	7.3×10^6	^c ...	3.7×10^{10}
Kepler 80 d	K	0.0372	2.4×10^{15}	2.1×10^6	^a ...	^a ...
HD 219134 b	K	0.03876	1.6×10^{14}	1.6×10^5	^b 0	^b 0
Kepler 21 b	F	0.0427	1.5×10^{15}	7.3×10^6	4.9×10^{21}	1.8×10^{10}
HD 219134c	K	0.0653	1.4×10^{14}	5.2×10^4	3.0×10^{20}	1.5×10^9
Pi Mensae c	G	0.06839	3.8×10^{15}	2.6×10^6	^b 0	^b 0
Kepler 100 b	G	0.0727	9.6×10^{13}	1.0×10^5	^a ...	^a ...
Kepler 105 c	G	0.0731	1.2×10^{15}	4.7×10^5	^a ...	^a ...
Kepler 36 b	G	0.1153	1.7×10^{14}	8.9×10^4	3.0×10^{18}	1.4×10^7

Notes.^a Cannot be calculated because H_{Tidal} is unknown (see Table 1).^b Equals 0 because $H_{\text{Tidal}} = 0$ (see Table 1).^c Unknown because atmospheric scale height, $H = kT_s/mg$, cannot be calculated (see Table 1).

less than the conservative end of estimates for Io's SO₂ column densities. While these calculations suggest that even in the absence of volcanism the extreme surface heating of close-in exoplanets may cause evaporation of their surfaces and outgassing, they also suggest that without abundant volcanism, all of the planets listed in Table 4 would have exospheres similar to Europa and Earth's moon rather than Io-like collisional atmospheres.

Constraining the expected tidally-driven volcanic outgassing rates and volcanic column densities, NO , for the rocky exoplanets in our study represents a novel approach to confirming their status as supervolcanic worlds. Thus we have also employed Equation (11) of Oza et al. (2019) to calculate the tidally-driven volcanic outgassing rates of several of the planets listed in Table 4, assuming that their atmospheres are dominated by SO₂. Thus their tidal efficiency, $\eta_T = H_{\text{Tidal}}/H_{\text{Tidal}_0}$. In addition we have employed Equation (5) of Oza et al. (2019) to determine the expected volcanic column densities of these planets, obtaining their scale heights, H , using the relation: $H = kT_s/mg$. Here $k = 1.38 \times 10^{-3} \text{ m}^2 \text{ kg s}^{-2} \text{ K}$ is Boltzmann's Constant, T_s is the exoplanet's surface temperature (Table 1), $m = 1.06 \times 10^{-25} \text{ kg}$ is the mass of one SO₂ molecule, and g is acceleration due to gravity (Table 1). H_{Tidal} for each exoplanet and H_{Tidal_0} are listed in Table 1. Based on the observations of Lellouch et al. (2015), Oza et al. (2019) concluded that the volcanic outgassing rate of SO₂ on Io is $\sim 6.9 \times 10^6 \text{ kg s}^{-1}$. Predicted tidally-driven volcanic outgassing

rates for SO₂ on 55 Cancri e, L 98-59 b & c, Kepler 21 b, HD 219134c, and Kepler 36 b would be between 1 and 8 orders of magnitude greater than this (Table 4). In addition, in the presence of strong tidal heating, volcanic column densities for 55 Cancri e, Kepler 21 b, HD 219134 c, and Kepler 36 b would be on the order of 10^{18} – 10^{25} molecules m⁻² (Table 4). These calculations suggest that these worlds experience very high levels of volcanic activity, due in large part to the tidal heating they experience because of their close-in, eccentric orbits. As is the case for Io, these exoplanets would also experience extreme loss of large amounts of volcanically-produced SO₂, S, and O which could lead to the production of Io-like collisional volcanic atmospheres. Even 55 Cancri e, which is categorized as a magma ocean world in Table 1, would have enough volcanic outgassing, because of its large tidal heating rate, to support a collisional atmosphere.

It must be reiterated that the above calculations are based on the assumptions that the rocky exoplanets in our study have atmospheres that are dominated by SO₂, and that SO₂ serves as the main volcanic volatile on these worlds. However, previous research has suggested that the atmosphere of 55 Cancri e is dominated by water vapor, N₂, CO₂, CO, or O₃ (Angelo & Hu 2017). Moreover, several volcanoes on Earth erupt carbon-rich lavas (Radebaugh et al. 2020), a phenomenon which could be pervasive on rocky exoplanets if extrasolar carbon planets are common throughout the galaxy (Kuchner & Seager 2005).

Thus, comparing expected SO_2 loss rates on extrasolar worlds with those on Io may not represent the most reliable method to confirm the supervolcanic status of the putative Super-Ios, Magma Ocean Worlds, etc., in our study. While we note that with careful consideration, the estimates provided above can be reformulated for CO_2 or other volcanic volatiles, an alternative approach that involves constraining the depth to magma layers in rocky exoplanets based on their surface temperatures, total internal heating rates, and the temperatures at which igneous rocks melt, may represent a more reliable way to confirm their status as supervolcanic worlds and discriminate between Super-Ios, Magma Ocean Worlds, and Exo-Venus Planets. Similar methods have been employed to determine the depth to subsurface oceans and liquid layers within the icy moons and TNOs in our solar system (Ruiz 2003; Quick & Marsh 2015; Saxena et al. 2018) and will be the focus of a future effort for the rocky exoplanets surveyed here.

Dorn et al. (2018) suggested that stagnant-lid planets with masses greater than $3M_{\oplus}$ would not have significant outgassing, while Noack et al. (2017) found that on stagnant-lid planets, outgassing only occurs on planets with masses below $4\text{--}7M_{\oplus}$. Furthermore, previous studies have suggested that the majority of volcanism on stagnant-lid planets occurs prior to 4.5 Gyr (Kite et al. 2009; Dorn et al. 2018). However, we find that even massive super-Earths, including 55 Cancri e, which is $8M_{\oplus}$, and ~ 10 Gyr old, are likely to be volcanically active. We also find that all of the Trappist planets, which have an upper limit age of 8 Gyr (Luger et al. 2017), will be volcanically or cryovolcanically active. Comparing calculated internal heating rates of each exoplanet in our study to the estimated internal heating rates of the planets and moons in our solar system indicates that all 53 exoplanets we considered are likely to exhibit moderate to extreme rates of volcanism at their surfaces. We find that the majority of exoplanets considered in this study are likely to exhibit volcanic activity at levels that are at least on par with, if not greater than, the most volcanically active bodies in our solar system. The agreement of our results with past studies that considered the magnitude of geological activity on exoplanets (e.g., Jackson et al. 2008; Barnes et al. 2010; Demory et al. 2015, 2016; Dobos et al. 2019) illustrates that the tidal heating rates obtained using Equation (1), and the radiogenic heating rates extracted from Frank et al. (2014), can be reliably employed to place conservative estimates on the expected magnitude of internal heating, and by extension, volcanic activity, on solid exoplanets. Hence from the standpoint of comparative exoplanetology, in which the internal heating rates and geological activity of the planets and moons in our solar system are used as a baseline, our results regarding the expected magnitude of volcanic activity on terrestrial exoplanets are robust.

Additionally, out of the 53 exoplanets that were surveyed, 14 ($\sim 26\%$) have effective temperatures and/or densities that are

consistent with them being candidate ocean planets. 9 out of these 14 planets ($\sim 64\%$) have effective temperatures and/or densities that are indicative of them being cold ocean planets. Hence, about 17% of all of the planets surveyed in this study may be cold ocean planets with internal structures that are similar to the moons of our solar system's giant planets (Figure 4), with similar geological activity at their surfaces. If conditions at the surfaces of candidate ocean planets Trappist-1b, Kepler 93 b, Kepler 138 c, Kepler 114 c, Kepler 80 e, LHS 1140c, Pi Mensae C and L98-59 d are such that they can maintain liquid water or high-pressure ices, then 21/53 or $\sim 40\%$ of the planets surveyed here may be ocean planets. Of note is that these totals do not include cold exoplanets such as OGLE 2005-BLG-390-Lb (Beaulieu et al. 2006), MOA-2007-BLG-192 (Bennett et al. 2008), or OGLE 2016-BLG-1195-Lb (Shvartzvald et al. 2017) which were detected by gravitational microlensing. These worlds may be cold ocean planets in their own rights, with ice-covered surfaces and internal oceans (Ehrenreich et al. 2006; Ehrenreich & Cassan 2007; Bond et al. 2017; Bourrier et al. 2017b). Depending on their total internal heating rates, they could also be geologically active. Our results suggest that a significant number of exoplanets that have been previously classified as terrestrial planets may instead be extrasolar oceans worlds that contain significant amounts of water and may exhibit cryovolcanism at their surfaces.

In our solar system, cryovolcanism on the moons of the giant planets serves as an important process that transports liquid water, energy and organics between their interiors and surfaces (Fagents 2003; Manga & Wang 2007; Lopes et al. 2013; Postberg et al. 2018b). In some cases, the circulation of cryomagmatic fluids could create transient habitable niches in the interiors of ice-covered worlds (Ruiz et al. 2007). In addition, recent studies have suggested that even planets that are mostly ice-covered may have substantial amounts of unfrozen land near their equators (Paradise et al. 2019) or small, equatorial regions of salt-rich water (del Genio et al. 2019) where life could flourish. The significant number of candidate cold ocean planets listed in Table 1 suggests that it is important to consider the possibility of habitable environments on planets that exist beyond the snowline in extrasolar planetary systems. Cryovolcanic eruptions on cold ocean planets could be detected by next-generation telescopes as transient or periodic excesses in H_2O , O_2 , and/or H in transit spectra that display spatial variability (Bourrier et al. 2017b; Quick et al. 2017a) or are localized to one hemisphere, as is the case for the cryovolcanically active moons in our solar system (Hurford et al. 2007; Hedman et al. 2013; Roth et al. 2014a, 2014b; Rhoden et al. 2015; Sparks et al. 2016, 2017; Teolis et al. 2017a, 2017b). If traces of cryovolcanic activity on exoplanets could be detected in transit spectra, this activity could be used as an indicator to determine which planets have substantial amounts of liquid water and internal energy, both of which are necessary ingredients for life.

We thank Dr. Orenthal Tucker for helpful discussions and an anonymous reviewer for helpful critiques that improved the quality of the manuscript.

Appendix

Determining Mantle Volumes for Ocean Planets

According to Schubert et al. (2009), Europa's mantle likely comprises 81% of its mass. Assuming that the densities of ice and silicates inside of Jupiter's moon Ganymede are 950 kg m^{-3} and 3500 kg m^{-3} , respectively, Equation (65) of Chen et al. (2014) reveals that the total mass of silicates within Ganymede is approximately $1 \times 10^{23} \text{ kg}$. If all of Ganymede's silicates are found within its mantle, then this suggests that Ganymede's mantle comprises 70% of its total mass. This information has been used to deduce that the mantles of Europa- and Ganymede-like planets comprise 69% and 40% of their total volumes, respectively, by employing the following procedure:

We know that $V_{\text{mantle}} = M_{\text{mantle}}/\rho_{\text{mantle}}$. If we assume that $\rho_{\text{Mantle}} = 3500 \text{ kg m}^{-3}$, we have for the case of Europa that:


$V_{\text{mantle}} = 0.81M_{\text{Europa}}/3500 \text{ kg m}^{-3} = (0.81 * 4.8 \times 10^{22} \text{ kg})/3500 \text{ kg m}^{-3} = 1.1 \times 10^{19} \text{ m}^3$. We can then employ the relationship:


$V_{\text{mantle}}/V_P = \frac{1.1 \times 10^{19} \text{ m}^3}{(4/3)\pi R_{\text{Europa}}^3} = \frac{1.1 \times 10^{19} \text{ m}^3}{(4/3)\pi [1.56 \times 10^6 \text{ m}]^3}$ to obtain $V_{\text{mantle}} = 0.69V_P$ for planets with Europa-like internal structures.


Similar steps may be taken to obtain $V_{\text{mantle}} = 0.4V_P$ for planets with Ganymede-like internal structures when we assume that the total mass of Ganymede's mantle is equivalent to the total mass of silicates in its interior so that $M_{\text{mantle}} = 1 \times 10^{23} \text{ kg} = 0.7M_{\text{Ganymede}}$.


From here, equations similar in form to Equations (2)–(4) were used to determine $H_{\text{Radiogenic}}$ in Table 2 for planets with internal structures that are more similar to our solar system's icy moons than to Earth.

ORCID iDs

Lynnae C. Quick  <https://orcid.org/0000-0003-0123-2797>

Aki Roberge  <https://orcid.org/0000-0002-2989-3725>

Amy Barr Mlinar  <https://orcid.org/0000-0001-5489-8934>

Matthew M. Hedman  <https://orcid.org/0000-0002-8592-0812>

References

- Abbot, D. S. 2016, *ApJ*, 827, 117
 Almenara, J. M., Díaz, R. F., Dorn, C., Bonfils, X., & Udry, S. 2018, *MNRAS*, 478, 460
 Anderson, J. D., Lau, E. L., Sjogren, W. L., Schubert, G., & Moore, W. B. 1996, *Natur*, 384, 541
 Anderson, J. D., Lau, E. L., Sjogren, W. L., Schubert, G., & Moore, W. B. 1997, *Sci*, 276, 1236
 Angelo, I., & Hu, R. 2017, *AJ*, 154, 232
 Arkhypov, O. V., Khodachenko, M. L., & Hansmeier, A. 2019, *A&A*, 631, A152
 Arnold, H., Liuzzo, L., & Simon, S. 2019, *GRL*, 46, 1149
 Arnold, H., Liuzzo, L., & Simon, S. 2020, *JGR Space Physics*, 125, e2019JA027346
 Barnes, R., Raymond, S. N., Greenberg, R., Jackson, B., & Kaib, N. A. 2010, *ApJL*, 709, L95
 Barr, A. C., Dobos, V., & Kiss, L. L. 2018, *A&A*, 613, A37
 Barros, S. C. C., Almenar, J. M., Deleuil, M., et al. 2014, *A&A*, 569, A74
 Basilevsky, A. T., Head, J. W., Schaber, G. G., & Strom, R. G. 1997, in *The Resurfacing History of Venus, Venus II*, ed. S. W. Bougher, D. M. Hunten, & R. J. Phillips (Tucson, AZ: The Univ. Arizona Press), 1047
 Beaulieu, J.-P., Bennett, D. P., Fouqué, P., et al. 2006, *Natur*, 439, 437
 Bennett, D. P., Bond, I. A., Udalski, A., et al. 2008, *ApJ*, 684, 663
 Berger, T. A., Huber, D., Gaidos, E., & van Saders, J. L. 2018, *ApJ*, 866, 99
 Berta-Thompson, Z. K., Irwin, J., Charbonneau, D., & Newton, E. R. 2015, *Natur*, 527, 204
 Bolmont, E., Selsis, F., Owen, J. E., et al. 2017, *MNRAS*, 464, 3728
 Bonati, I., Lichtenberg, T., Bower, D. J., Timpe, M. L., & Quanz, S. P. 2019, *A&A*, 621, A125
 Bond, I. A., Bennett, D. P., Sumi, T., et al. 2017, *MNRAS*, 469, 2434
 Bondarenko, N. V., Head, J. W., & Ivanov, M. A. 2010, *GeoRL*, 37, L23202
 Bonfils, X., Almenara, J.-M., Cloutier, R., et al. 2018, *A&A*, 618, A142
 Bonomo, A. S., Sozzetti, A., Lovis, C., et al. 2014, *A&A*, 572, A2
 Borg, L., & Drake, M. J. 2005, *JGRE*, 110, E12S03
 Borsato, L., Marzari, F., Nascimbeni, V., et al. 2014, *A&A*, 571, A38
 Borucki, W. J., Agol, E., Fressin, F., et al. 2013, *Sci*, 340, 587
 Borucki, W. J., Koch, D. G., Basri, G., et al. 2011, *ApJ*, 728, 117
 Bourrier, V., de Wit, J., Bolmont, E., et al. 2017b, *AJ*, 154, 121
 Braden, S. E., Stopar, J. D., Robinson, M. S., et al. 2014, *NatGe*, 7, 787
 Breuer, D., Hauck, S. A., Buske, M., Pauer, M., & Spohn, T. 2007, *SSRv*, 132, 229
 Brossier, J. F., Gilmore, M. S., & Toner, K. 2020, *Icar*, 343, 113693
 Bydko, M. I. 1969, *Tell*, 21, 611
 Běhouňková, M., Tobie, G., Cadek, O., et al. 2015, *NatGe*, 8, 601
 Carey, S., & Bursik, M. 2015, in *Volcanic Plumes. Encyclopedia of Volcanoes*, ed. H. Sigurdsson (New York: Academic), 571
 Carter, J. A., Agol, E., Chaplin, W. J., et al. 2012, *Sci*, 337, 556
 Cassen, P., Reynolds, R. T., & Peale, S. J. 1979, *GeoRL*, 6, 731
 Cassidy, T. A., Mendez, R., Arras, P., Johnson, R. E., & Skrutskie, M. F. 2009, *ApJ*, 704, 1341
 Castillo-Rogez, J. C., Hesse, M. A., Formisano, M., et al. 2019, *GeoRL*, 46, 1963
 Charpinet, S., Fontaine, G., Brassard, P., et al. 2011, *Natur*, 480, 496
 Chen, E. M. A., Nimmo, F., & Glatzmaier, G. A. 2014, *Icar*, 229, 11
 Christiansen, J. L., Vanderburg, A., Burt, J., et al. 2017, *AJ*, 154, 122
 Cioni, R., & Pistolesi, M. R. 2015, in *Plinian and Subplinian Eruptions. Encyclopedia of Volcanoes*, ed. H. Sigurdsson (New York: Academic), 519
 Cook, J. C., Desch, S. J., Roush, T. L., Trujillo, C. A., & Geballe, T. R. 2007, *ApJ*, 663, 1406
 Crawford, G. D., & Stevenson, D. J. 1988, *Icar*, 73, 66
 Croft, S. K., Kargel, J. S., Kirk, R. L., et al. 1995, in *The Geology of Triton. Neptune and Triton*, ed. D. P. Cruikshank (Tucson, AZ: Univ. Arizona Press), 895
 Davies, A. G., Keszthelyi, L. P., & Harris, A. J. L. 2010, *JVGR*, 194, 75
 de Kleer, K., de Pater, I., Molter, E. M., et al. 2019a, *AJ*, 158, 29
 de Kleer, K., Nimmo, F., & Kite, E. 2019b, *GeoRL*, 46, 6327
 Dean, K. G., Dehn, J., Papp, K. R., et al. 2004, *JVGR*, 135, 51
 del Genio, A. D., Way, M. J., Amundsen, D. S., et al. 2019, *AsBio*, 19, 99
 Demory, B.-O., Gillon, M., Deming, D., et al. 2011, *A&A*, 533, A114
 Demory, B.-O., Gillon, M., de Wit, J., et al. 2016, *Natur*, 532, 207
 Demory, B.-O., Gillon, M., & Madhusudhan, N. 2015, *MNRAS*, 455, 2018
 Dittmann, J. A., Irwin, J. M., Charbonneau, D., Berta-Thompson, Z. K., & Newton, E. R. 2017a, *AJ*, 154, 142
 Dittmann, J. A., Irwin, J. M., Charbonneau, D., & Bonfils, X. 2017b, *Natur*, 544, 333
 Dobos, V., Barr, A. C., & Kiss, L. L. 2019, *A&A*, 624, A2
 Dorn, C., Noack, L., & Rozel, A. B. 2018, *A&A*, 614, A18
 Dressing, C. D., Charbonneau, D., Dumusque, X., & Gette, S. 2015, *ApJ*, 800, 135
 Driscoll, P. E., & Barnes, R. 2015, *AsBio*, 15, 739
 Ehrenreich, D., & Cassan, A. 2007, *AN*, 328, 789

- Ehrenreich, D., Lecavelier des Etangs, A., Beaulieu, J.-P., & Grasset, O. 2006, *ApJ*, 651, 535
- Elkins-Tanton, L. 2012, *AREPS*, 40, 113
- Esteves, L. J., de Mooij, E. J. W., & Jayawardhana, R. 2015, *ApJ*, 804, 150
- Everett, M. E., Barclay, T., Ciardi, D. R., et al. 2015, *AJ*, 149, 55
- Fabrycky, D. C., Lissauer, J. J., Ragozzine, D., et al. 2014, *ApJ*, 790, 146
- Fagents, S. A. 2003, *JGRE*, 108, 5139
- Fagents, S. A., Greeley, R., Sullivan, R. J., Pappalardo, R. T., & Prockter, L. M. 2000, *Icar*, 144, 54
- Filiberto, J., Trang, D., Treiman, A. H., & Gilmore, M. S. 2020, *SciA*, 6, eaax7445
- Frank, E. A., Meyer, B. S., & Mojzsis, S. J. 2014, *Icar*, 243, 274
- Fu, R., O'Connell, R. J., & Sasselov, D. D. 2010, *ApJ*, 708, 1326
- Fu, R. R., Ermakov, A. I., Marchi, S., et al. 2017, *E&PSL*, 476, 153
- Fulton, B. J., & Petigura, E. A. 2018, *AJ*, 156, 264
- Gaeman, J., Hier-Majumder, S., & Roberts, J. H. 2012, *Icar*, 220, 339
- Garraffo, C., Drake, J. J., Cohen, O., Alvarado-Gómez, J. D., & Moschou, S. P. 2017, *ApJL*, 843, L33
- Garry, W. B., Robinson, M. S., Zimbelman, J. R., et al. 2012, *JGRE*, 117, E00H31
- Geissler, P. E. 2015, in *Cryovolcanism in the Outer Solar System*. Encyclopedia of Volcanoes, ed. H. Sigurdsson (New York: Academic), 763
- Giardini, D., Lognonné, P., Banerdt, W. B., et al. 2020, *NatGe*, 13, 205
- Gillon, M., Demory, B.-O., van Grootel, V., et al. 2017a, *NatAs*, 1, 0056
- Gillon, M., Triaud, A. H. M. J., Demory, B.-O., et al. 2017b, *Natur*, 542, 456
- Goldreich, P., & Soter, S. 1966, *Icar*, 5, 375
- Gozdziewski, K., Migaszewski, C., Panichi, F., & Szuszkiewicz, E. 2016, *MNRAS*, 455, L104
- Guenther, E. W., Cabrera, J., Erikson, A., et al. 2011, *A&A*, 525, A24
- Guenther, E. W., & Kislyakova, K. G. 2020, *MNRAS*, 491, 3974
- Hadden, S., & Lithwick, Y. 2014, *ApJ*, 787, 80
- Hamano, K., Kawahara, H., Abe, Y., Onishi, M., & Hashimoto, G. L. 2015, *ApJ*, 806, 216
- Hammond, N. P., Barr, A. C., & Parmentier, E. M. 2016, *GeoRL*, 43, 6775
- Harris, A. J. L., & Rowland, S. K. 2015, in *Lava Flows and Rheology*, Encyclopedia of Volcanoes, ed. H. Sigurdsson (New York: Academic), 321
- Hauck, S. A., Dombard, A. J., Phillips, R. J., & Solomon, S. C. 2004, *E&PSL*, 222, 713
- Head, J. W., Crumpler, L. S., & Aubele, J. C. 1992, *JGR*, 97, 13153
- Head, J. W., Pappalardo, R. T., Kay, J., et al. 1998, *Cryovolcanism on Ganymede: Evidence in Bright Terrain from Galileo Solid State Imaging Data*. 29th Lunar and Planetary Science Conf. (Houston, TX: Lunar and Planetary Institute), Abstract #1666
- Hedman, M. M., Gosmeyer, C. M., Nicholson, P. D., et al. 2013, *Natur*, 500, 182
- Henning, W. G., & Hurford, T. A. 2014, *ApJ*, 789, 30
- Henning, W. G., Renaud, J. P., Saxena, P., et al. 2018, arXiv:1804.05110
- Howett, C. J. A., Spencer, J. R., Pearl, J., & Segura, M. 2011, *JGRE*, 116, E03003
- Huang, C. X., Burt, J., Vanderburg, A., et al. 2018, *ApJL*, 868, L39
- Hurford, T. A., Helfenstein, P., Hoppa, G. V., Greenberg, R., & Bills, B. G. 2007, *Natur*, 447, 292
- Hurford, T. A., Henning, W. G., Maguire, R., et al. 2020, *Icar*, 338, 113466
- Hussmann, H., Sohl, F., & Spohn, T. 2006, *Icar*, 185, 258
- Hussmann, H., & Spohn, T. 2004, *Icar*, 171, 391
- Ikoma, M., Elkins-Tanton, L., Hamano, K., & Suckale, J. 2018, *SSRv*, 214, 76
- Jackson, B., Barnes, R., & Greenberg, R. 2008, *MNRAS*, 391, 237
- Jacobson, R. A., Campbell, J. K., Taylor, A. H., & Synnott, S. P. 1992, *AJ*, 103, 2068
- Jia, X., Kivelson, M. G., Khurana, K. K., & Kurth, W. S. 2018, *NatAs*, 2, 459
- Jin, S., & Mordasini, C. 2018, *ApJ*, 853, 163
- Johnson, R. E., Oza, A., Young, L. A., Volkov, A. N., & Schmidt, C. 2015, *ApJ*, 809, 43
- Jontof-Hutter, D., Ford, E. B., Rowe, J. F., et al. 2016, *ApJ*, 820, 39
- Kadoya, S., & Tajika, E. 2014, *ApJ*, 790, 107
- Kaltenegger, L., Henning, W. G., & Sasselov, D. D. 2010, *AJ*, 140, 1370
- Kamata, S., Nimmo, F., Sekine, Y., et al. 2019, *NatGe*, 12, 407
- Kattenhorn, S. A., & Hurford, T. 2009, in *Tectonics of Europa*. Europa, ed. R. T. Pappalardo, W. B. McKinnon, & K. Khurana (Tucson, AZ: Univ. Arizona Press), 199
- Kay, J. E., & Head, J. W., III 1999, in *Geologic Mapping of the Ganymede G8 Calderas Region: Evidence for Cryovolcanism?* 30th Lunar and Planetary Science Conf. (Houston, TX: Lunar and Planetary Institute), Abstract #1103
- Khodachenko, M. L., Ribas, I., Lammer, H., et al. 2007, *AsBio*, 7, 167
- Kirchoff, M. R., Bierhaus, E. B., Dones, L., et al. 2018, in *Cratering Histories in the Saturnian System*. Enceladus and the Icy Moons of Saturn, ed. P. M. Schenk et al. (Tucson, AZ: Univ. Arizona Press), 267
- Kislyakova, K. G., Fossati, L., Johnstone, C. P., et al. 2018, *ApJ*, 858, 105
- Kislyakova, K. G., Fossati, L., Shulyak, D., et al. 2019, arXiv:1907.05088
- Kislyakova, K. G., Noack, L., Johnstone, C. P., et al. 2017, *NatAs*, 1, 878
- Kite, E. S., Fegley, B., Schaefer, L., & Ford, E. B. 2020, *ApJ*, 891, 111
- Kite, E. S., Manga, M., & Gaidos, E. 2009, *ApJ*, 700, 1732
- Kostov, V. B., Schlieder, J. E., Barclay, T., et al. 2019, *AJ*, 158, 32
- Kozai, Y. 1968, *BGeod*, 89, 355
- Kuchner, M. J. 2003, *ApJL*, 596, L105
- Kuchner, M. J., & Seager, S. 2005, *Extrasolar Carbon Planets*, arXiv:astro-ph/0504214v2
- Kumar, S. 1979, *Natur*, 280, 758
- Lammer, H., Odert, P., Leitzinger, M., et al. 2009, *A&A*, 506, 399
- Léger, A., Grasset, O., Fegley, B., et al. 2011, *Icar*, 213, 1
- Léger, A., Selsis, F., Sotin, C., et al. 2004, *Icar*, 169, 499
- Lellouch, E., Ali-Dib, M., Jessup, K.-L., et al. 2015, *Icar*, 253, 99
- Lellouch, E., Belton, M., de Pater, I., et al. 1992, *Icar*, 98, 271
- Lellouch, E., Strobel, D. F., Belton, M. J., et al. 1996, *ApJL*, 459, L107
- Levi, A., Sasselov, D., & Podolak, M. 2013, *ApJ*, 769, 29
- Levi, A., Sasselov, D., & Podolak, M. 2014, *ApJ*, 792, 125
- Lissauer, J. J., Jontof-Hutter, D., Rowe, J. F., et al. 2013, *ApJ*, 770, 131
- Livingston, J. H., Crossfield, I. J. M., Petigura, E. A., et al. 2018, *AJ*, 156, 277
- Lognonné, P., Banerdt, W. B., Pike, W. T., et al. 2020, *NatGe*, 13, 213
- Lopes, R. M. C., Kamp, L. W., Smythe, W. D., et al. 2004, *Icar*, 169, 140
- Lopes, R. M. C., Kirk, R. L., Mitchell, K. L., et al. 2013, *JGRE*, 118, 416
- Lopes, R. M. C., & Williams, D. A. 2015, in *Volcanism on Io*. Encyclopedia of Volcanoes, ed. H. Sigurdsson (New York: Academic), 747
- López-Morales, M., Haywood, R. D., Coughlin, J. L., & Zeng, L. 2016, *AJ*, 152, 204
- Luger, R., Sestovic, M., Kruse, E., et al. 2017, *NatAs*, 1, 0129
- MacDonald, M. G., Ragozzine, D., Fabrycky, D. C., et al. 2016, *AJ*, 152, 105
- Makarov, V. V., Berghea, C. T., & Efroimsky, M. 2018, *ApJ*, 857, 142
- Makarov, V. V., & Efroimsky, M. 2014, *ApJ*, 795, 7
- Manga, M., & Wang, C.-Y. 2007, *GeoRL*, 34, L07202
- Manga, M., Zhai, G., & Wang, C.-Y. 2019, *GeoRL*, 46, 6333
- Marcy, G. W., Isaacson, H., Howard, A. W., et al. 2014, *ApJS*, 2010, 20
- Massol, H., Hamano, K., Tian, F., et al. 2016, *SSRv*, 205, 153
- McEwen, A. S., Kesztelyi, L. P., Lopes, R., Schenk, P. M., & Spencer, J. R. 2004, in *The Lithosphere and Surface of Io*. Jupiter: The Planet, Satellites, and Magnetosphere, ed. F. Bagenal, T. Dowling, & W. McKinnon (New York: Cambridge Univ. Press), 307
- McGrath, M. A., Lellouch, E., Strobel, D. F., Feldman, P. D., & Johnson, R. E. 2004, in *Satellite Atmospheres*. Jupiter: The Planet, Satellites, and Magnetosphere, ed. F. Bagenal, T. Dowling, & W. McKinnon (New York: Cambridge Univ. Press), 457
- McKinnon, W. B., Nimmo, F., Wong, T., et al. 2016, *Natur*, 534, 82
- Ment, K., Dittmann, J. A., Astudillo-Defru, N., et al. 2019, *AJ*, 157, 32
- Meyer, J., Elkins-Tanton, L., & Wisdom, J. 2010, *Icar*, 208, 1
- Meyer, J., & Wisdom, J. 2007, *Icar*, 188, 535
- Mills, S. M., Howard, A. W., Weiss, L. M., et al. 2019, *AJ*, 157, 145
- Misra, A., Krissansen-Totten, J., Koehler, M. C., & Sholes, S. 2015, *AsBio*, 15, 462
- Miyamoto, H., Mitri, G., Showman, A. P., & Dohm, J. M. 2005, *Icar*, 177, 413
- Moore, W. B. 2003, *JGR*, 108, 5096
- Moore, W. B., & Schubert, G. 2003, *Icar*, 166, 223
- Mordasini, C. 2020, *A&A*, in press
- Morton, T. D., Bryson, S. T., Coughlin, J. L., et al. 2016, *ApJ*, 882, 86
- Muirhead, P. S., Johnson, J. A., Apps, K., et al. 2012, *ApJ*, 747, 144
- Neveu, M., & Desch, S. J. 2015, *GeoRL*, 42, 10197

- Neveu, M., & Rhoden, A. R. 2019, *NatAs*, 3, 543
- Nimmo, F., Hamilton, D. P., McKinnon, W. B., et al. 2016, *Natur*, 540, 94
- Nimmo, F., Spencer, J. R., Pappalardo, R. T., & Mullen, M. E. 2007, *Natur*, 447, 289
- Noack, L., Godolt, M., von Paris, P., et al. 2014, *P&SS*, 98, 14
- Noack, L., Höning, D., Rivoldini, A., et al. 2016, *Icar*, 277, 215
- Noack, L., Rivoldini, A., & van Hoolst, T. 2017, *PEPI*, 269, 40
- Ogawa, M. 2016, *JGRE*, 121, 118
- Ojakangas, G. W., & Stevenson, D. J. 1989, *Icar*, 81, 220
- Owen, J. E., & Wu, Y. 2017, *ApJ*, 847, 29
- Oza, A. V., Johnson, R. E., Lellouch, E., et al. 2019, *ApJ*, 885, 168
- Paganini, L., Villanueva, G. L., Roth, L., et al. 2019, *NatAs*, 4, 266
- Paige, D. A., & Siegler, M. A. 2016, in *New Constraints on Lunar Heat Flow Rates from LRO Diviner Lunar Radiometer Experiment Polar Observations. 47th Lunar and Planetary Science Conf. (Houston, TX: Lunar and Planetary Institute)*, Abstract #2753
- Paradise, A., Menou, K., Valencia, D., & Lee, C. 2019, *JGRE*, 124, 1
- Parfitt, E. A., & Wilson, L. 2008, *Fundamentals of Physical Volcanology (USA: Blackwell Science Ltd.)*, 77
- Parro, L. M., Jiménez-Díaz, A., Mansilla, F., & Ruiz, J. 2017, *NatSR*, 7, 45629
- Parro, L. M., Ruiz, J., & Pappalardo, R. T. 2016, *P&SS*, 130, 24
- Peale, S. J., Cassen, P., & Reynolds, R. T. 1979, *Sci*, 203, 892
- Pepe, F., Collier Cameron, A., Latham, D. W., & Molinari, E. 2013, *Natur*, 503, 377
- Peplowski, P. N., Evans, L. G., Hauck, S. A., II, et al. 2011, *Sci*, 333, 1850
- Phillips, C. B., McEwen, A. S., Hoppa, G. V., et al. 2000, *JGR*, 105, 22579
- Porco, C. C., Helfenstein, P., Thomas, P. C., et al. 2006, *Sci*, 311, 1393
- Postberg, F., Clark, R. N., Hansen, C. J., et al. 2018a, in *Plume and Surface Composition of Enceladus. Enceladus and the Icy Moons of Saturn*, ed. R. N. Clark et al. (Tucson, AZ: Univ. Arizona Press), 129
- Postberg, F., Kempf, S., Schmidt, J., et al. 2009, *Natur*, 459, 1098
- Postberg, F., Khawaja, N., Abel, B., et al. 2018b, *Natur*, 558, 564
- Prockter, L. M., & Patterson, G. W. 2009, in *Morphology and Evolution of Europa's Ridges and Bands. Europa*, ed. R. T. Pappalardo, W. B. McKinnon, & K. Khurana (Tucson, AZ: Univ. Arizona Press), 237
- Prockter, L. M., Shirley, J. H., Dalton, J. B., III, & Kamp, L. 2017, *Icar*, 285, 27
- Qiao, L., Head, J., Wilson, L., et al. 2017, *Geo*, 45, 455
- Queloz, D., Bouchy, F., Moutou, C., et al. 2009, *A&A*, 506, 303
- Quick, L. C., Adams, E., & Barr, A. C. 2017a, in *Prospects for Detecting Cryovolcanic Activity in Exoplanetary Systems. Planetary Science Vision 2050 Workshop (Houston, TX: Lunar and Planetary Institute)*, Abstract #8036
- Quick, L. C., Barnouin, O. S., Prockter, L. M., & Patterson, W. G. 2013, *P&SS*, 86, 1
- Quick, L. C., Buczkowski, D. B., Ruesch, O., et al. 2019, *Icar*, 320, 119
- Quick, L. C., Glaze, L. S., & Baloga, S. M. 2017b, *Icar*, 284, 477
- Quick, L. C., & Hedman, M. M. 2020, *Icar*, 343, 113667
- Quick, L. C., & Marsh, B. D. 2015, *Icar*, 253, 16
- Quick, L. C., & Roberge, A. 2018, in *The Potential for Volcanism and Tectonics on Extrasolar Terrestrial Planets. 231st Meeting of the American Astronomical Society (Washington, DC: American Astronomical Society)*, Paper # 439.21
- Quintana, E. V., Barclay, T., Raymond, S. N., & Rowe, J. F. 2014, *Sci*, 344, 277
- Radebaugh, J., Barnes, R., & Keith, J. 2020, in *The Ol Doinyo Lengai Volcano, Tanzania, as an Analog For Carbon Planets. Exoplanets in Our Backyard Meeting (Lunar and Planetary Institute, Houston, TX)*, Abstract #3070
- Ramirez, R., & Kaltenegger, L. 2017, *ApJL*, 837, L4
- Rathbun, J. A., Tate, C. D., Corlies, P., Hayes, A., & Spencer, J. R. 2019, in *Io's Loki Volcano: An Explanation of its Tricky Behaviour and Prediction for the Next Eruption. EPSC-DPS Joint Meeting 13, EPSC-DPS2019-769-1*
- Rhoden, A. R., Henning, W., Hurford, T. A., Patthoff, D. A., & Tajeddine, R. 2017, *JGRE*, 122, 400
- Rhoden, A. R., Hurford, T. A., Roth, L., & Retherford, K. 2015, *Icar*, 253, 169
- Roberts, J. H., & Nimmo, F. 2008, *Icar*, 194, 675
- Robuchon, G., & Nimmo, F. 2011, *Icar*, 216, 426
- Rogers, L. A. 2015, *ApJ*, 801, 41
- Roth, L., Retherford, K. D., Saur, J., et al. 2014a, *PNAS*, 111, E5123
- Roth, L., Saur, J., Retherford, K. D., et al. 2014b, *Sci*, 343, 171
- Ruiz, J. 2003, *Icar*, 166, 436
- Ruiz, J., Montoya, L., López, V., & Amils, R. 2007, *OLEB*, 37, 287
- Sagan, C., & Mullen, G. 1972, *Sci*, 177, 52
- Sasaki, S., & Nakazawa, K. 1986, *JGRB*, 91, 9231
- Saxena, P., Elkins-Tanton, L., Petro, N., & Mandell, A. 2017, *E&PSL*, 474, 198
- Saxena, P., Renaud, J. P., Henning, W. G., Jutzi, M., & Hurford, T. 2018, *Icar*, 302, 245
- Scharf, C. A. 2006, *ApJ*, 648, 1196
- Schenk, P., & Jackson, M. P. A. 1993, *Geo*, 21, 299
- Schenk, P. M., McKinnon, W. B., Gwynn, D., & Moore, J. M. 2001, *Natur*, 410, 57
- Schubert, G., Anderson, J. D., Spohn, T., & McKinnon, W. B. 2004, in *Interior Composition, Structure and Dynamics of the Galilean Satellites. Jupiter: The Planet, Satellites, and Magnetosphere*, ed. F. Bagenal, T. Dowling, & W. McKinnon (New York: Cambridge Univ Press), 281
- Schubert, G., Sohl, F., & Hussmann, H. 2009, in *Interior of Europa. Europa*, ed. R. T. Pappalardo, W. B. McKinnon, & K. Khurana (Tucson, AZ: Univ. Arizona Press), 353
- Schubert, G., Solomatov, V. S., Tackley, P. J., & Turcotte, D. L. 1997, in *Mantle Convection and Thermal Evolution of Venus. Venus II*, ed. S. W. Bougher, D. M. Hunten, & R. J. Phillips (Tucson, AZ: The Univ. Arizona Press), 1245
- Schubert, G., Spohn, T., & Reynolds, R. T. 1986, in *Thermal Histories, Compositions, and Internal Structures of the Moons of the Solar System. Satellites*, ed. J. Burns & M. Matthews (Tucson, AZ: Univ. Arizona Press), 224
- Sellers, W. D. 1969, *JApMe*, 8, 392
- Shalygin, E. V., Markiewicz, W. J., Basilevsky, A. T., et al. 2015, *GeoRL*, 42, 4762
- Showman, A. P., Mosqueira, I., & Head, J. W., III 2004, *Icar*, 172, 625
- Shvartzvald, Y., Yee, J. C., Novati, S. C., et al. 2017, *ApJL*, 840, L3
- Siegler, M. A., & Smrekar, S. E. 2014, *JGRE*, 119, 47
- Smrekar, S. E., Stofan, E. R., Mueller, N., et al. 2010, *Sci*, 328, 605
- Sori, M. M., & Bramson, A. M. 2019, *GeoRL*, 46, 1222
- Sotin, C., Grasset, O., & Mocquet, A. 2007, *Icar*, 191, 337
- Sparks, W. B., Hand, K. P., McGrath, M. A., et al. 2016, *ApJ*, 829, 121
- Sparks, W. B., Schmidt, B. E., McGrath, M. A., et al. 2017, *ApJL*, 839, L18
- Spencer, J. R., Barr, A. C., Esposito, L. W., et al. 2009, in *Enceladus: An Active Cryovolcanic Satellite. Saturn from Cassini-Huygens*, ed. M. K. Dougherty, L. W. Esposito, & S. M. Krimigis (New York: Springer), 683
- Spencer, J. R., Rahtbun, J. A., Travis, L. D., et al. 2000, *Sci*, 288, 1198
- Spencer, J. R., Stern, S. A., Cheng, A. F., et al. 2007, *Sci*, 218, 240
- Stacey, F. D., & Davis, P. M. 2008, *Physics of the Earth (Cambridge: Cambridge Univ. Press)*
- Stassun, K. G., Collins, K. A., & Gaudi, B. S. 2017, *AJ*, 153, 136
- Stevenson, D. J. 1982, *P&SS*, 30, 755
- Stevenson, D. J. 2003, *CRGeo*, 335, 99
- Taddeucci, J., Edmonds, M., Houghton, B., James, M. R., & Vergnolle, S. 2015, in *Hawaiian and Strombolian Eruptions. Encyclopedia of Volcanoes*, ed. H. Sigurdsson (New York: Academic Press), 485
- Tajika, E. 2008, *ApJL*, 680, L53
- Tamburo, P. 2018, in *Observational Evidence of Possible Volcanic Activity on an Extrasolar Planet. American Geophysical Union Fall Meeting (Washington, DC: American Geophysical Union)*, Abstract #P44A-07B
- Tamburo, P., Mandell, A., Deming, D., & Garhart, E. 2018, *AJ*, 155, 221
- Teolis, B. D., Perry, M. E., Hansen, C. J., et al. 2017a, *AsBio*, 17, 926
- Teolis, B. D., Wyrick, D. Y., Bouquet, A., Magee, B. A., & Waite, J. H. 2017b, *Icar*, 284, 18
- Thomas, P. C., Tajeddine, R., Tiscareno, M. S., et al. 2016, *Icar*, 264, 37
- Tobie, G., Cadek, O., & Sotin, C. 2008, *Icar*, 196, 642
- Tonks, W., & Melosh, J. 1993, *JGRE*, 98, 5319
- Torres, G., Kipping, D. M., Fressin, F., & Caldwell, D. A. 2015, *ApJ*, 800, 99
- Trowbridge, A. J., Melosh, H. J., Steckloff, J. K., & Freed, A. M. 2016, *Natur*, 534, 79
- Turcotte, D. L. 1995, *JGR*, 100, 16931

- Turcotte, D. L., & Schubert, G. 2002, *Geodynamics* (2nd ed.; New York: Cambridge Univ. Press)
- Vance, S., Barnes, R., Brown, J. M., et al. 2015, in *Interior Structure and Habitability of Super-Europas and Super-Ganymedes*. 46th Lunar and Planetary Science Conf. (Houston, TX: Lunar and Planetary Institute), Abstract# 2717
- Vance, S., Bouffard, M., Choukroun, M., & Sotin, C. 2014, *P&SS*, 96, 62
- Vance, S., Hammeijer, J., Kimura, J., et al. 2007, *AsBio*, 7, 987
- Veeder, G. J., Matson, D. L., Johnson, T. V., Blaney, D. L., & Goguen, J. D. 1994, *JGR*, 99, 17095
- von Braun, K., Boyajian, T. S., ten Brummelaar, T. A., et al. 2011, *ApJ*, 740, 49
- Wang, S., Wu, D.-H., Barclay, T., & Laughlin, G. P. 2017, arXiv:1704.04290
- Watters, T. R., Weber, R. C., Collins, G. C., et al. 2019, *NatGe*, 12, 411
- Williams, J.-P., Paige, D. A., Greenhagen, B. T., & Sefton-Nash, E. 2017, *Icar*, 283, 300
- Wolf, E. T. 2017, *ApJL*, 839, L1
- Xie, J.-W. 2014, *ApJS*, 210, 25
- Yang, J., Ding, F., Ramirez, R. M., et al. 2017, *NatGe*, 10, 556
- Yoder, C. F., & Peale, S. J. 1981, *Icar*, 47, 1